MAGNETICALLY STEERED CELL THERAPY FOR FUNCTIONAL RESTORATION OF INTRAOCULAR PRESSURE CONTROL IN OPEN-ANGLE GLAUCOMA

M. Reza Bahrani Fard[1], Jessica Chan[2], A. Thomas Read[3], Guorong Li[4], Lin Cheng[5,6], Babak N. Safa[3], Seyed Mohammad Siadat[3], Anamik Jhunjhunwala[3], Hans E. Grossniklaus[7], Stanislav Y. Emelianov[3,8], W. Daniel Stamer[4], Markus H. Kuehn[5,6], C. Ross Ethier[1,3]

1. Woodruff School of Mechanical Engineering, Georgia Institute of Technology, Atlanta, Georgia
2. School of Chemistry and Biochemistry, Georgia Institute of Technology, Atlanta, Georgia
3. Wallace H. Coulter Department of Biomedical Engineering, Georgia Institute of Technology/Emory University, Atlanta, Georgia
4. Department of Ophthalmology, Duke University, Durham, NC
5. Departments of Ophthalmology and Visual Sciences, The University of Iowa, Iowa City, IA
6. Veterans Administration Center for the Prevention and Treatment of Visual Loss, Iowa City VA Healthcare System, Iowa City, IA
7. Departments of Ophthalmology and Pathology, Emory University School of Medicine, Atlanta, GA
8. School of Electrical and Computer Engineering, Georgia Institute of Technology, Atlanta, Georgia
9. Departments of Ophthalmology and Biomedical Engineering, Duke University, Durham, NC

Corresponding author:

C. Ross Ethier, Ph.D.

Professor and Georgia Research Alliance Eminent Scholar in Bioengineering

Wallace H. Coulter Department of Biomedical Engineering

Georgia Institute of Technology/Emory University

ross.ethier@bme.gatech.edu

1. Abstract

Trabecular meshwork (TM) cell therapy has been proposed as a next-generation treatment for elevated intraocular pressure (IOP) in glaucoma, the most common cause of irreversible blindness. Using a magnetic cell steering technique with excellent efficiency and tissue-specific targeting, we delivered two types of cells into a mouse model of glaucoma: either human adipose-derived mesenchymal stem cells (hAMSCs) or induced pluripotent cell derivatives (iPSC-TM cells). We observed a 4.5 [3.1, 6.0] mmHg or 27% reduction in intraocular pressure (IOP) for nine months after a single dose of only 1500 magnetically-steered hAMSCs, associated with restoration of function to the conventional outflow pathway, as judged by increased outflow facility and TM cellularity. iPSC-TM cells were also effective, but less so, showing only a 1.9 [0.4, 3.3] mmHg or 13% IOP reduction and increased risk of tumorigenicity. In both cases, injected cells remained detectable in the iridocorneal angle three weeks post-transplantation. Based on the locations of the delivered cells, the mechanism of IOP lowering is most likely paracrine signaling. We conclude that magnetically-steered hAMSC cell therapy has potential for long-term treatment of ocular hypertension in glaucoma.

One Sentence Summary: A novel magnetic cell therapy provided effective intraocular pressure control in a mouse model of glaucoma, motivating future translational studies.

2. Introduction

Glaucoma, an optic neuropathy, is the leading cause of irreversible blindness, with more than 80 million cases worldwide *(1)*. Primary open-angle glaucoma (POAG), the most common subtype of the disease, is characterized by a gradual loss of retinal ganglion cells and a corresponding loss of vision. While the exact mechanism underlying retinal ganglion loss is not well understood, elevated intraocular pressure (IOP) is a major risk factor *(2)*; consequently, all current clinical treatments seek to sustainably lower IOP, using pharmacological, laser, and surgical means. However, the success of such IOP-lowering treatments is reduced by low patient adherence to medical therapies *(3)*, by post-surgical complications, and/or by patients becoming refractory to originally successful treatments *(4)*. Thus, there remains a major unmet public health need for methods that offer sustained IOP control in glaucoma patients.

The trabecular meshwork (TM; Figure 1A) is an ocular tissue that drains the majority of aqueous humor (AH) from the human eye, and its function is a major determinant of IOP. There are a number of age- and glaucoma-associated changes in the TM, including an age-associated loss

of TM cells which is accelerated in POAG *(5)*. This cell deficiency has been identified as a therapeutic target for IOP control in glaucoma patients, with multiple groups attempting to re-functionalize the TM by injection of stem cells into the eye to restore normal IOP homeostasis *(6–14)*.

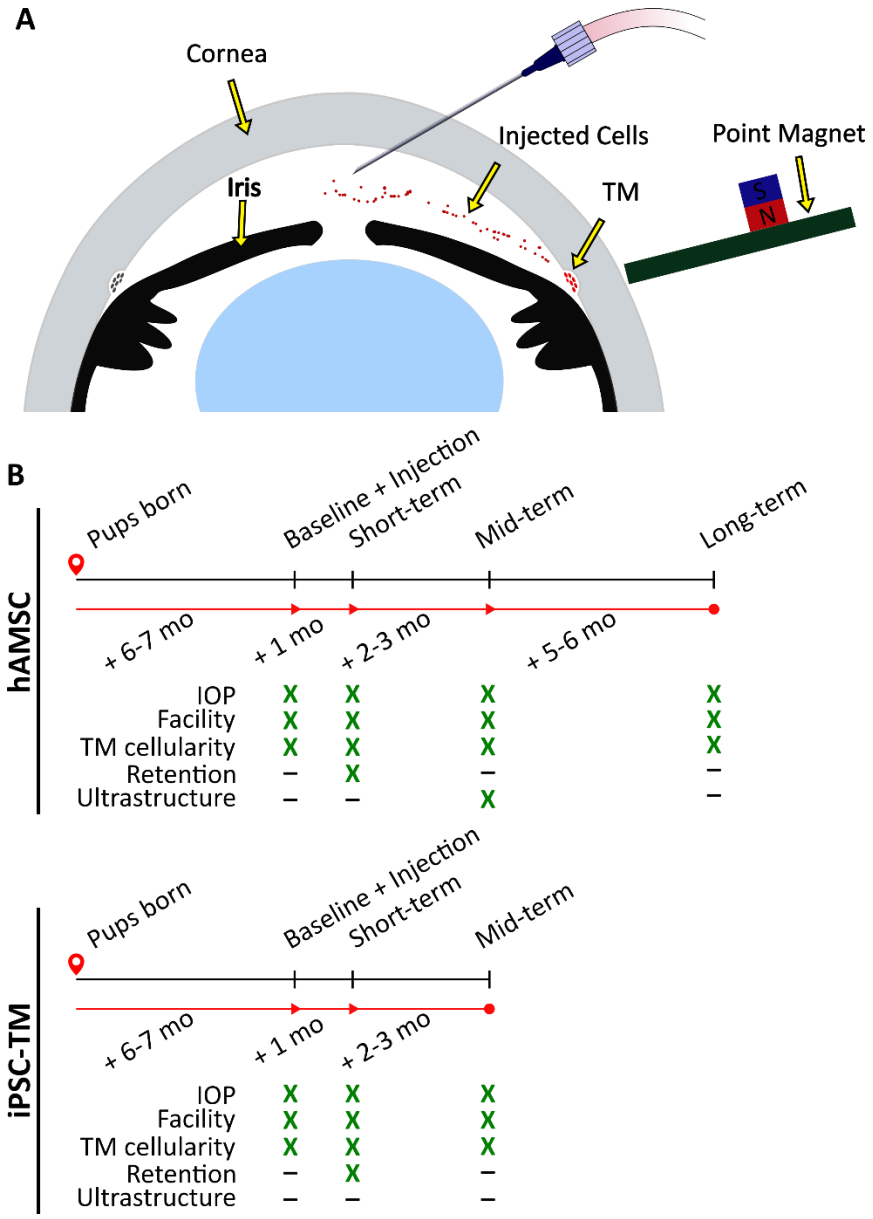

Figure 1. Experimental schematic and design. A) Schematic of magnetically-steered cell delivery to the TM. As cells are injected into the anterior chamber at a low flow rate, the experimenter places the "point magnet" *(15)* on the limbus and carefully drags the cells towards the iridocorneal angle, targeting the trabecular meshwork (TM). Features of the figure are not drawn to scale. B) Time-line of the experiments. An ultrastructural analysis, specifically the quantification of inner wall basement membrane fenestrations, was not undertaken for eyes receiving iPSC-TMs due to their inferior performance. Additionally, cell retention in the anterior chamber was only

investigated at the short-term. Note that baseline measurements were taken for WT and transgenic animals that did not necessarily receive an injection afterwards. Refer to Methods for a description of various experimental groups and further details.

Despite the potential of stem cell treatment for IOP control, there remain several critical barriers to translation. For example, cell delivery to the TM has typically relied on passive transport of cells by AH outflow, leading to extremely low delivery efficiencies *(16)*. A more efficient delivery method is desirable, which is expected to both increase the therapeutic benefit of the treatment and reduce immunogenicity; for example, Zhou et al. reported an increase in the inflammatory markers CD45 and GR1 and T-cell markers CD4 and CD3 in the iris and the cornea after mesenchymal stem cell injection, likely due to off-target cell delivery *(13)*. We have recently introduced a magnetically-steered cell delivery technique which significantly outperforms previously-used magnetic and non-magnetic delivery techniques *(15)*. Here we characterize the efficacy of our stem cell delivery using this technique to lower IOP.

A second barrier to translation is lack of knowledge about which cell type should be delivered to restore TM function. Three types of cells have previously been used in this context: native TM stem cells (TMSC), mesenchymal stem cells, and induced pluripotent stem cell (iPSC) derivatives. TMSC therapy lowers IOP and increases TM cellularity *(11, 14)*, and is theoretically attractive. However, the scarcity of TMSCs, constituting only 2-5% of the entire TM cell population *(17)*, and the invasiveness of the required cell collection procedure significantly reduce the translational potential of this cell source. Alternatively, mesenchymal stem cells have been used in several studies, showing a transient IOP reduction as well as neuroprotection *(6, 7)*. For example, Manuguerra-Gagné et al. injected bone-marrow derived mesenchymal stem cells in a rat model of IOP elevation, observing a reduction in IOP for three weeks *(6)*. These results, together with the ease of sourcing autologous cells, and the established safety of mesenchymal stem cell therapy in clinical trials *(18, 19)*, make these stem cells a strong candidate for clinical POAG cell therapy. Finally, iPSCs can be differentiated into iPSC-TM cells, with the differentiated cells displaying phenotypic similarity to adult TM cells *(20)*. Intracameral injection of iPSC-TMs into a perfused porcine anterior segment POAG model restored the IOP homeostatic response *(8)*. Additionally, Zhu and colleagues delivered iPSC-TMs into the anterior chambers of ocular hypertensive mice and reported increased TM cellularity due to proliferation of endogenous cells and a corresponding decrease in the IOP for up to 12 weeks after cell delivery *(9, 10)*. Although both MSC and IPSC-TM showed promise, there is no information about their efficacy and safety

in comparison to each other. Therefore, here we compare the benefits of mesenchymal stem cells vs. iPSC-TM cells.

An additional barrier to translation is the choice of an appropriate animal model for preclinical testing, since no animal model replicates all the pathological phenotypes of POAG. For example, although non-human primate models show high anatomical and functional resemblance to humans and are the gold standard for certain pre-clinical studies *(21)*, induction of ocular hypertension requires laser photocoagulation of the TM, which is very unlike TM changes seen in POAG *(6, 22)*. Microbead *(23)* and hypertonic saline *(24)* models of ocular hypertension are similarly distinct from human POAG pathology. Commercially available DBA/2 mice show TM cell loss and IOP elevation but are associated with undesirable systemic and ocular complications *(25)*. Thus, in this work we chose to use transgenic $MYOC^{Y437H}$ mice. These mice carry a glaucoma-causing point mutation in the MYOC gene, and have been reported to show an accelerated loss of TM cellularity and a gradual ocular hypertension development *(26)*.

In summary, we here evaluate the effectiveness of TM cell therapy, using a magnetic cell steering method and two clinically relevant cell choices, namely human adipose-derived mesenchymal stem cells (hAMSCs) and iPSC-TM cells, in $MYOC^{Y437H}$ mice. We judged effectiveness by the extent and longevity of IOP reduction, improvement in outflow facility, and increase in TM cellularity, among other outcome measures, and performed experiments using animal cohorts at different time points (Figure 1 B, detailed in Methods section). Our data demonstrate a sustained IOP lowering and a significant benefit of magnetic cell steering in the eye, particularly for hAMSCs, strongly indicating further translational potential.

3. Results

a. Cell transplantation lowered IOP and improved aqueous humor dynamics

We delivered and magnetically steered either hAMSCs or iPSC-TMs to the TM into eyes of $MYOC^{Y437H}$ mice (Figure 1 A), measuring IOPs and outflow facilities at short-, mid-, and long-term time points, corresponding to ~1 month, 3-4 months, and 9 months after cell delivery (Figure 1 B). Our high-level goals were to: (i) elucidate the impact of hAMSC or iPSC-TM delivery on IOP; and (ii) quantify the portion of IOP change due to changes in outflow facility, a key functional metric of the TM. Outflow facility is the numerical inverse of the hydraulic resistance to aqueous humor drainage through the conventional outflow pathway.

We expected transgenic MYOC^{Y437H} mice to show elevated IOP by 6-7 months of age, when baseline IOP measurements were taken *(9, 10, 26)*. Surprisingly, we saw no meaningful IOP difference between Tg-MYOC^{Y437H} mice (Tg group) vs. wild-type littermates (Figure 2; Table 1 and Table 2). Despite this lack of IOP elevation in the transgenic model, magnetically-steered delivery of hAMSCs led to a marked IOP decrease in Tg animals as compared to sham injection of saline at short-, mid-, and, long-term time points. The IOP reduction was sustained in hAMSC-treated eyes over all three time points, with no statistically significant difference between any combination of these time points. iPSC-TM treatment also led to a reduction in IOP compared to sham (phosphate-buffered saline, PBS) injection controls at both the short-and mid-term time points, although this difference did not reach statistical significance at the latter time. The IOP reduction due to iPSC-TM cells was approximately half that due to hAMSC treatment at both short- and medium-term time points (short term: $-4.3\ [-5.6, -2.9]\ \mathrm{mmHg}$ for hAMSC vs. $-2.3[-3.6, -1.0]\ \mathrm{mmHg}$ for iPSC-TM, $p = 0.021$; mid-term: $-4.5\ [-5.8, -3.1]\ \mathrm{mmHg}$ for hAMSC vs. $-1.9\ [-3.3, -0.4]\ \mathrm{mmHg}$ for iPSC-TM, $p = 0.005$; all data reported as means and 95% confidence intervals).

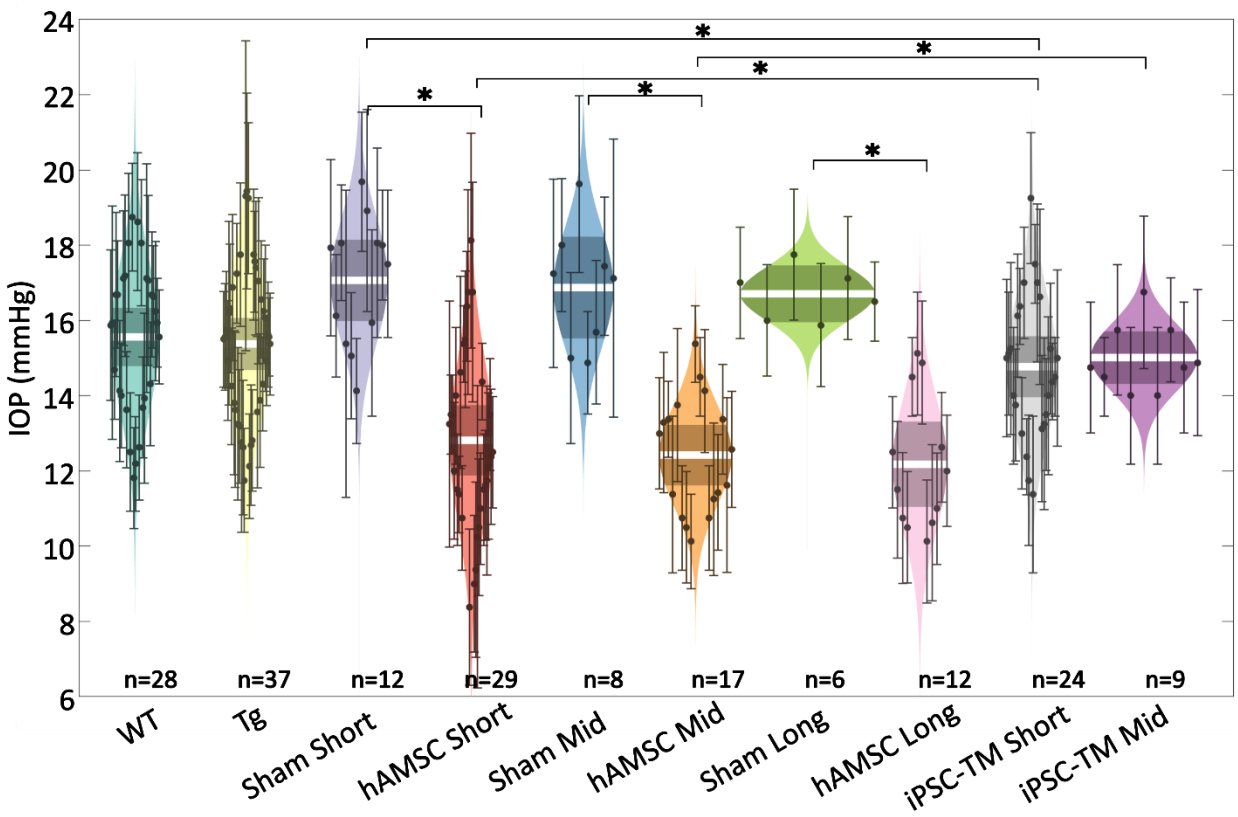

Figure 2. IOP was reduced by targeted cell delivery to the TM. In each experimental cohort, the central white strip indicates the mean, while the darker region represents the 95% confidence

interval on the mean. The colored region shows the distribution. Dots represent individual eyes, with error bars demarcating the 95% confidence intervals. For further information on experimental groups and statistical analysis refer to text. *$p < 0.05$ with Bonferroni correction (see Table 2). See below for a more complete statistical analysis. WT: wildtype hybrid mice (naïve control), Tg: Tg- MYOCY437H mice, Sham: Tg mice receiving saline injection, hAMSC: Tg mice receiving magnetically-steered hAMSCs, iPSC-TM: Tg mice receiving magnetically-steered iPSC-TMs. “Short”, "Mid”, and “Long” refer to time points. n is number of eyes measured in each group.

We observed increases in outflow facility for eyes receiving stem cells which were consistent with observed changes in IOP (Figure 3 A-B; Table 1 and Table 2). Specifically, no significant difference in facility was found between the naïve wildtype (WT) and transgenic groups, while hAMSC treatment led to a marked increase in outflow facility vs. injection (sham) controls at short-, mid- and long-term time points. Further, the percentage increases in facility due to hAMSC delivery vs. sham injection controls were similar at all time points. Groups receiving iPSC-TMs also showed an increase in facility, but these differences did not reach statistical significance. Specifically, hAMSC delivery led to a significantly higher percentage increase in facility compared to iPSC-TM delivery (short-term: $170\ [70, 310]\%$ for hAMSC vs. $40\ [-10, 110]\%$ for iPSC-TM, $p = 0.011$; mid-term: $180\ [110, 280]\%$ for hAMSC vs. $40\ [0, 110]\%$ for iPSC-TM, $p = 0.003$; data reported as percent increase in treatment group compared to relevant (sham) injection control).

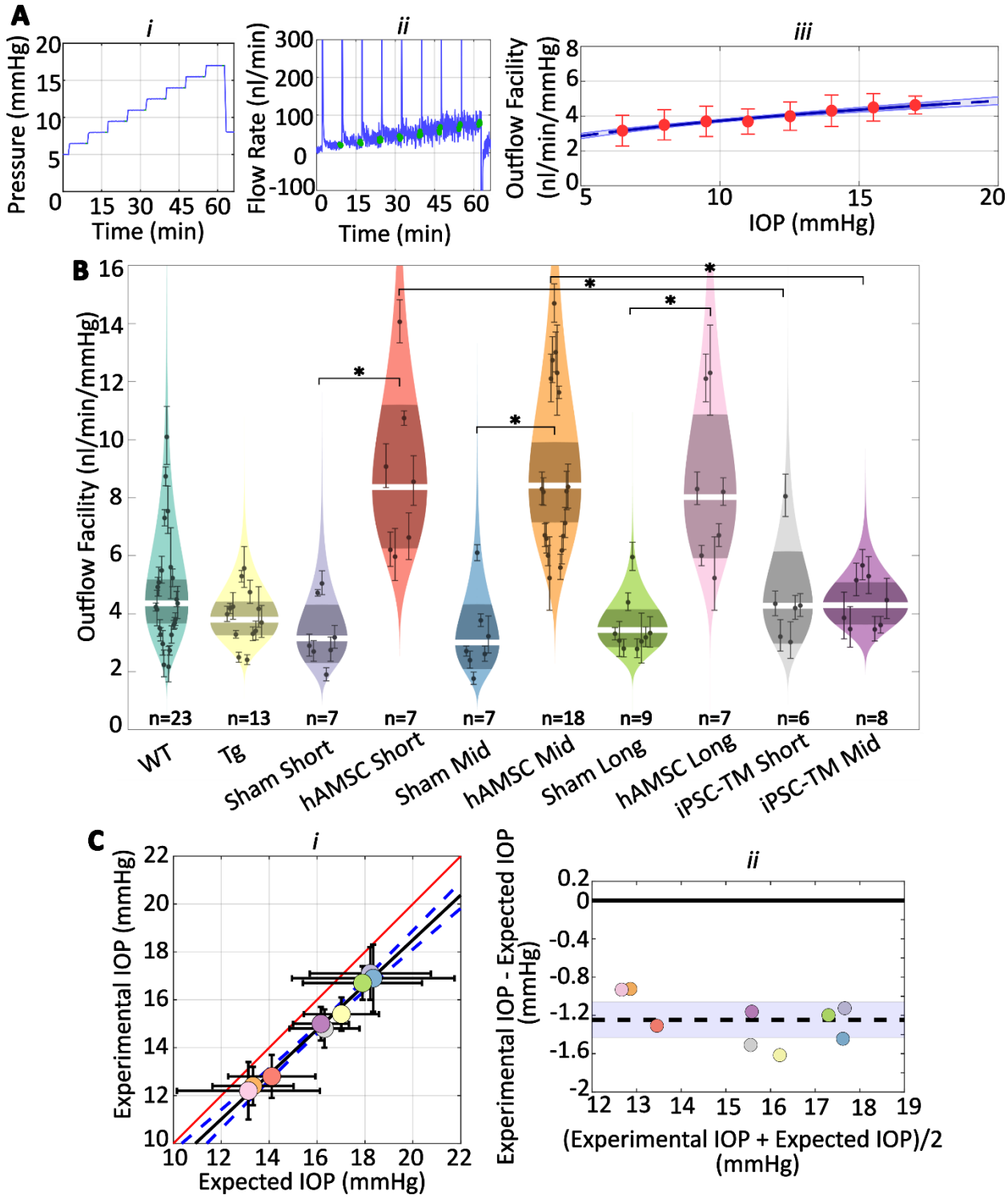

Figure 3. hAMSCs increase outflow facility in mice. **A** i-ii) IOP and flow rate vs. time for multiple pressure steps during the perfusion experiment in a representative eye. After each pressure step, the perfusion system automatically waits for a steady state inflow rate to be achieved, based on the criterion that the rate of change in the inflow rate falls below 3 nl/min/min. The steady intervals for each step are shown in green. Data has been trimmed to not include preparatory and pre-

loading phases. **A** iii) Calculated outflow facility (red dots) vs. IOP. The solid curve shows the fitted model with the shaded region being the 95% confidence interval on the regression line. Error bars are 95% confidence intervals on individual steps. **B)** Outflow facilities across different experimental cohorts. Refer to Figure 2 for interpretation details. Note that outflow facilities in mice follow a log-normal distribution. **C)** Cross-validation of experimentally-measured and expected IOP, calculated from measured facility values. i) Regression plot of experimental vs. expected IOPs. Solid black fitted line ($y = 0.94x - 0.21,\ R^2 = 0.99$) is shown along with its confidence bounds in dashed blue. Error bars show 95% confidence interval on both experimental (vertical) and expected (horizontal) IOPs. The unity line is shown as a solid red line. ii) Bland-Altman plot of IOP residuals (experimental minus expected IOPs) vs. average of experimental and expected IOPs. Individual experimental groups are indicated by colors matching those in panel B. Dashed line is shows the mean and is shown along with its 95% confidence interval (shaded). Solid line shows zero difference between the two parameters, i.e. the null hypothesis. For further information on experimental groups and statistical analysis refer to text. $*\ p < 0.05$ with Bonferroni correction (see Table 2).

We then asked whether the measured decreases in IOP were quantitatively consistent with the experimentally-measured increases in outflow facility. To answer this question, we used the modified Goldmann equation *(27)*, which relates IOP to facility and other variables, computing an "expected" IOP from the facility measurements for each cohort of mice. Comparison of this expected IOP with the actual (measured) IOP showed a close correlation (Figure 3 C*i*), determined by linear regression (slope of fitted line was not statistically different from one, $p = 0.22$, $R^2 = 0.99$). Still, the outflow facility measurements overestimated the actual IOP by a small amount ($1.2\ [1.1, 1.3]\ \mathrm{mmHg}$, $p < 10^{-6}$, null hypothesis: average difference between experimental and expected IOPs equals zero, Figure 3 C*ii*). Despite this "shift" between the experimentally-measured and expected IOP, the horizontal error bars in Figure 3 C*i*, derived by a propagation of error analysis, include the unity line for all groups, suggesting that the small discrepancy between the two experimental and expected values falls within the measurement errors (see Discussion).

b. Cell delivery increased TM cellularity

The observed reductions in IOP and increases in outflow facility after delivery of both cell types suggested restoration of function to the conventional outflow pathway. We therefore asked whether these changes were associated with alteration of the cellular density in the TM by evaluating cell counts in histological sections of the iridocorneal angle from all of our experimental groups (Figure 4; Table 1 and Table 2). We observed more nuclei in eyes receiving cell transplantation, with a striking 2.2-fold increase in TM cellularity (normalized to the anterior-posterior length of the outflow tissues) after hAMSC treatment at the short-term time point vs. the corresponding (sham) injection control (Figure 4 C). Interestingly, this spike in TM cell density was followed by a decline over time, reaching a 1.6-fold increase at the mid-term time point, and

apparently plateauing at 1.6-fold at the long-term time point. Despite this modest decline, hAMSC-treated eyes showed significantly higher cellular density vs. their injection controls at both mid-term and long-term time points.

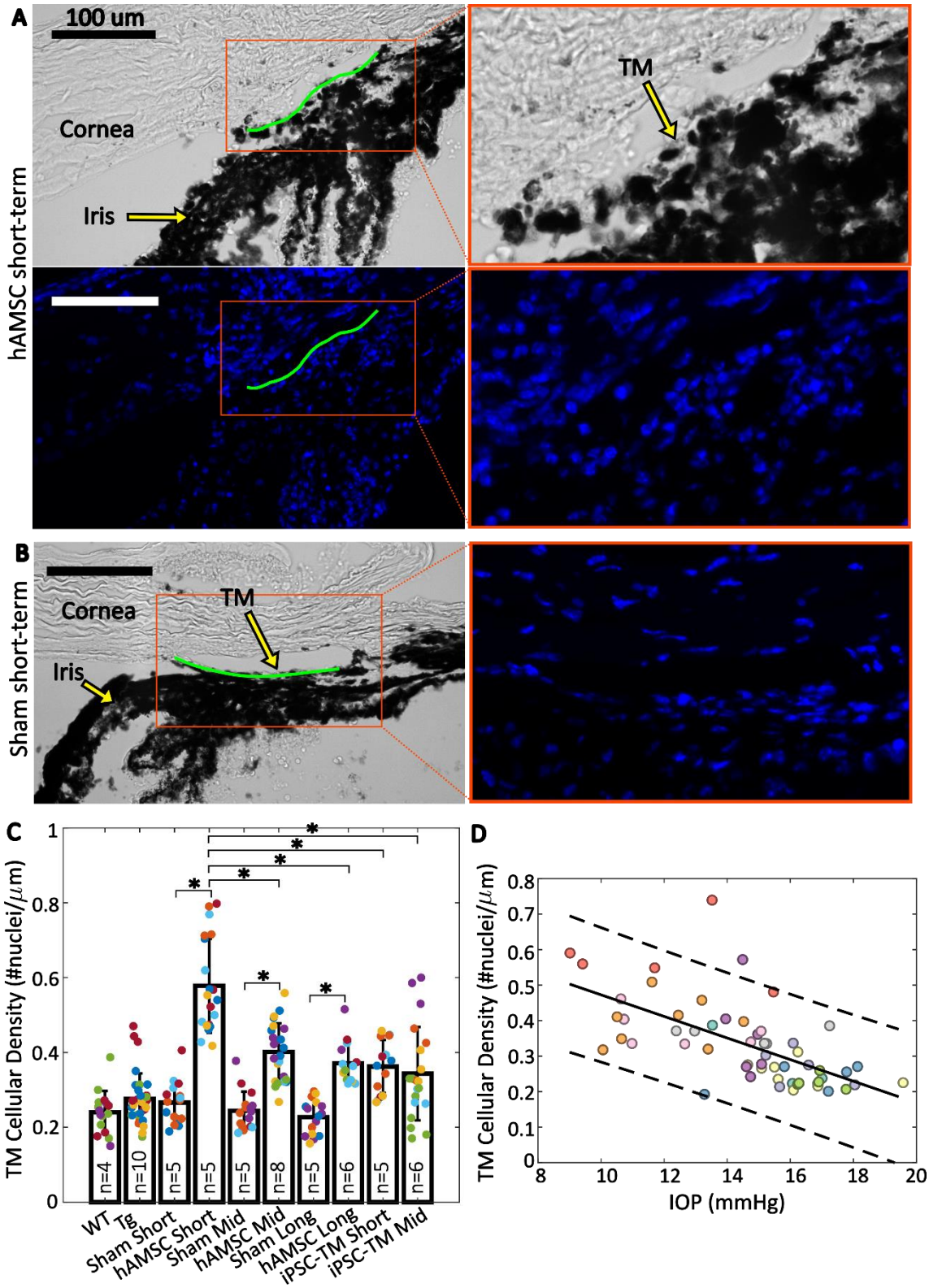

Figure 4. TM cellular density is improved by stem cell delivery. **A** and **B)** Brightfield and fluorescent micrographs of the irideocorneal angle (sagittal view) taken from a representative eye from the iPSC-TM short-term **(A)** and sham short-term **(B)** experimental groups. Green line shows the

contour of the TM along the inner wall of Schlemm's Canal used for normalizing nuclei count. DAPI-stained nuclei in the fluorescent image are shown in blue. Adjacent panels show a magnified view of the angle. **C)** Comparison of TM cellular density (number of nuclei per length of inner wall of Schlemm's canal) for various experimental cohorts. Bars show mean and standard deviation. Multiple sections analyzed from each eye are coded with the same color. n = number of eyes. Linear mixed-effect model, $*p < 0.05$ with Bonferroni correction (see Table 2). **D)** Cross-comparison of TM cellularity vs. IOP for the eyes shown in panel **C**. The negative correlation between the variables was statistically confirmed (Pearson correlation coefficient = -0.63 and $p < 10^{-7}$). Each color represents one eye, with different colors matching the experimental groups shown in Figure 2. Trend line (solid) is shown along with the 95% prediction interval (dashed).

Delivery of iPSC-TMs also led to an increase in TM cellular density vs. (sham) injection controls at both short-term and mid-term time points, although these differences were more modest than seen in hAMSC-injected eyes and did not reach statistical significance. Interestingly, the TM cellular densities in iPSC-TM-treated eyes at both time points were comparable to those at the mid-term and long-term time points in hAMSC-treated eyes but were significantly different than hAMSC-treated eyes at the short-term time point.

Cross-plotting normalized TM cellularity vs. IOP for pooled data from all the experimental groups (Figure 4D) showed a strong negative correlation between these two parameters, indicating an association between greater TM cellularity and lower IOP.

c. hAMSC transplantation significantly decreased basement membrane material

An increased deposition of extracellular matrix (ECM), and in particular basement membrane material (BMM), in the TM immediately adjacent to the inner wall (IW) of Schlemm's canal has been associated with ocular hypertension *(28, 29)*. Since this region within the TM accounts for the majority of AH outflow resistance *(30)*, we asked whether the amount of BMM was altered by stem cell treatment. To address this question we compared the mid-term hAMSC transplanted group vs. its corresponding injection control (Figure 5), selecting the mid-term time point for this analysis since this was the longest time point previously studied *(10)* and we were interested in persistent ECM changes within the TM.

Reduced amounts of BMM adjacent to the inner wall of Schlemm's canal were evident in transmission electron micrographs from eyes receiving hAMSCs compared to sham-injected controls at the mid-term time point (Figure 5A). Quantification showed that stem cell treatment significantly decreased the amount of BMM, as determined by the ratio of BMM length adjacent to Schlemm's canal inner wall to total inner wall length; specifically, this ratio was 0.52 [0.34, 0.70]

in sham-treated eyes vs. 0.34 [0.22, 0.47] in hAMSC-treated eyes ($p < 0.0001$). The BMM length ratio was measured by two independent annotators (MRB, CRE), and differences between the annotators were not significant (annotator considered as a random effect, $p \approx 1$, likelihood ratio test).

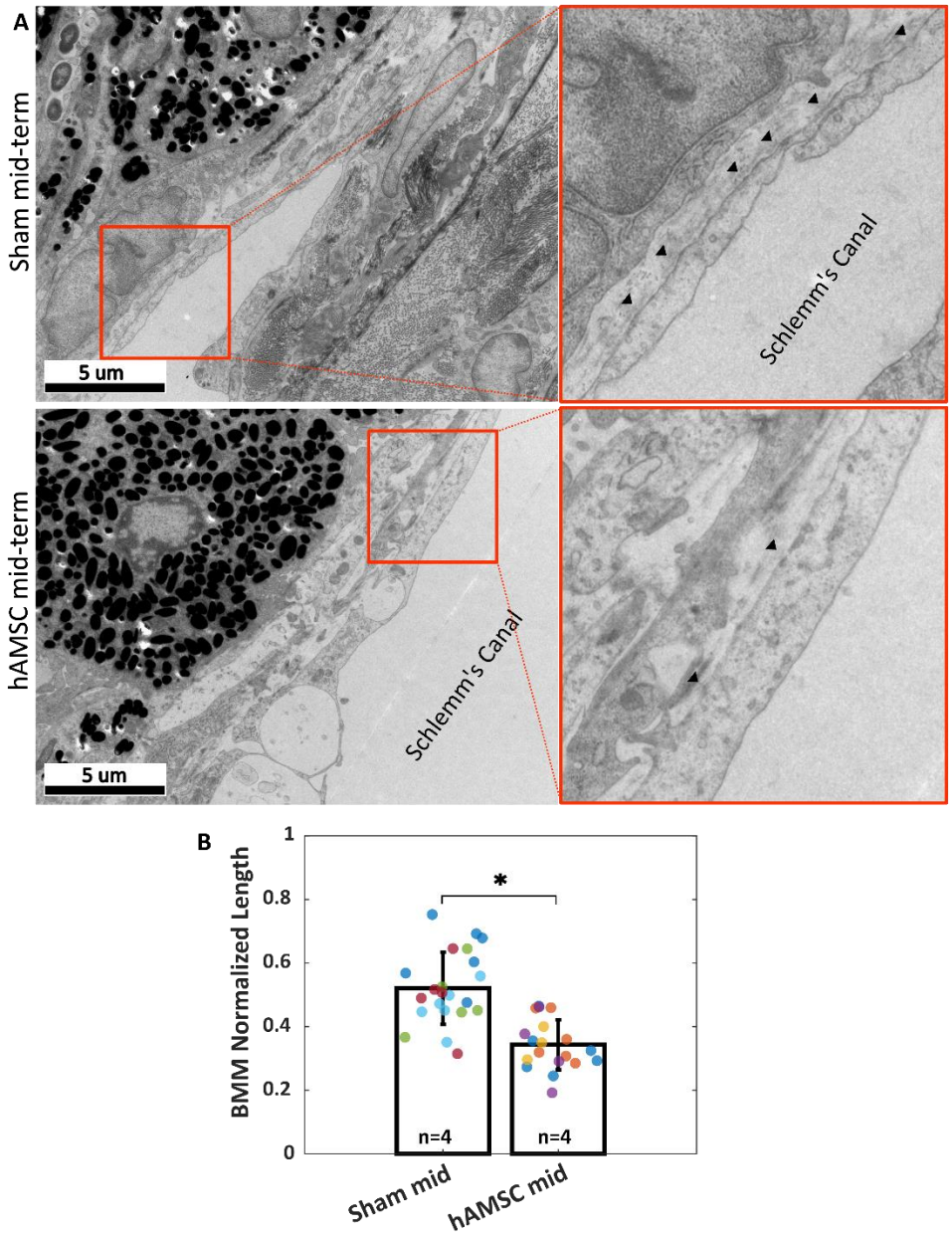

Figure 5. Ultrastructural analysis of ECM underlying the inner wall of Schlemm's canal (basement membrane material, or BMM). A) Greater amounts of BMM are evident immediately adjacent to the inner wall of Schlemm's canal (arrowheads) in a saline-injected eye (top row) vs. in a hAMSC-treated eye (bottom row) at the mid-term time point. The images at right are a zoomed view of the orange boxed areas in the left panels. B) The normalized length of BMM directly in contact with

the IW (length of BMM material divided by length of inner wall of Schlemm's canal) for the experimental groups represented in panel A. Dots represent the average value between annotators for each measured section. Multiple sections analyzed from each eye are coded with the same color. n = number of eyes. Linear mixed-effect model. $*\, p < 0.05$.

d. Exogenous cells were retained for multiple weeks in the TM

Manuguerra-Gagné et al. previously reported a surprisingly low retention duration of hAMSCs in the TM of rat eyes, with virtually no fluorescently-labeled exogenous cells being present in histological sections four days after injection *(6)*. We therefore pre-labelled injected cells with PKH26 fluorescent dye, which allowed us to track cells for up to 3 weeks after injection. *En face* images showed a relatively uniform distribution of cells over the entire circumference of the eye (Figure 6A), similar to previous results with magnetically steered cells *(15)*. Sagittal sections (Figure 6B) showed an accumulation of exogenous cells deep within the iridocorneal angle. Interestingly, strong fluorescent signals were observed within the TM in iPSC-TM-injected eyes, indicating cell integration with the target tissue; in contrast, most hAMSCs accumulated close to the TM (within $\sim 50\ \mu m$), but did not enter the TM. Note that fluorescent signals observed in the posterior part of the eye and outside the eye near the limbus were caused by autofluorescence (supplementary Supplementary Figure 3).

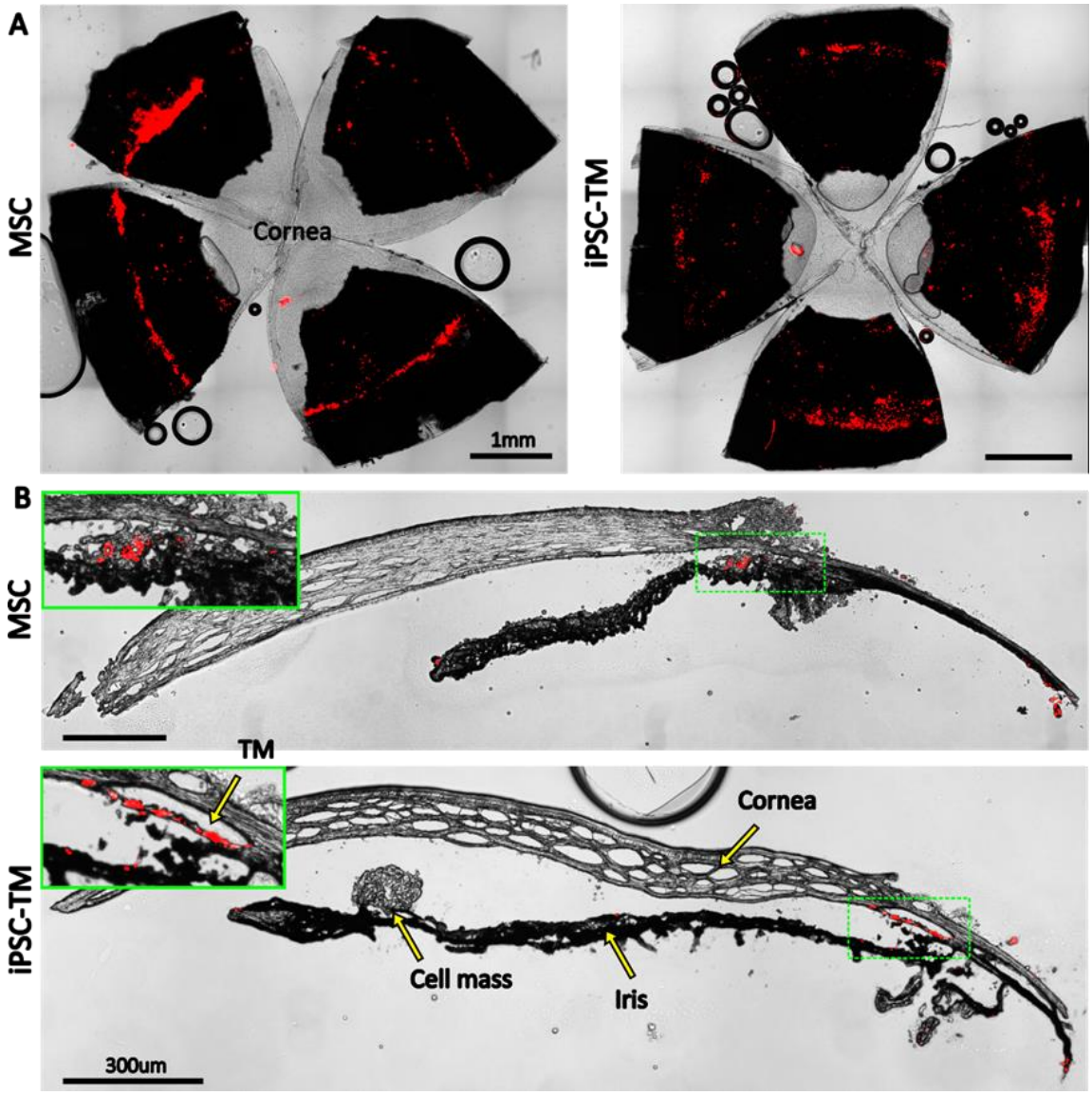

Figure 6. Retention of exogenous cells in the anterior segment 3 weeks after injection. Distribution of both hAMSC and iPSC-TM cells (red) are shown in A) *en face* images of the anterior segments and B) sagittal sections. In panel B), insets show a magnified view of the sites with the most intense fluorescent signal (green boxes). Autofluorescence can be seen in the posterior chambers as well as exterior to the corneoscleral shell. A cell mass, possibly a growing tumor, can be seen over the iris in the iPSC-TM injected eye.

e. iPSC-TM transplantation led to significant incidence of tumor formation

Unfortunately, there was a very high rate of tumorigenicity in eyes receiving iPSC-TMs, with more than 60% of eyes showing large intraocular masses within a month of cell injection, typically on the iris (Figure 6B). In most cases these tumors left the eyes unusable for IOP or outflow facility measurements. Examination of select iPSC-TM-transplanted sections by a board-certified

pathologist (HEG) confirmed the presence of tumors (Figure 7), based on observation of rosettes and neuroectodermal phenotype, characteristics also found in various tumor types, including retinoblastoma *(31)*. Additionally, a high nuclear-cytoplasmic ratio, a hallmark of tumor malignancy *(32)*, and rarefaction due to tissue necrosis were noted. No signs of tumor growth were observed in the eyes injected with hAMSCs at the long-term time point (Figure 7).

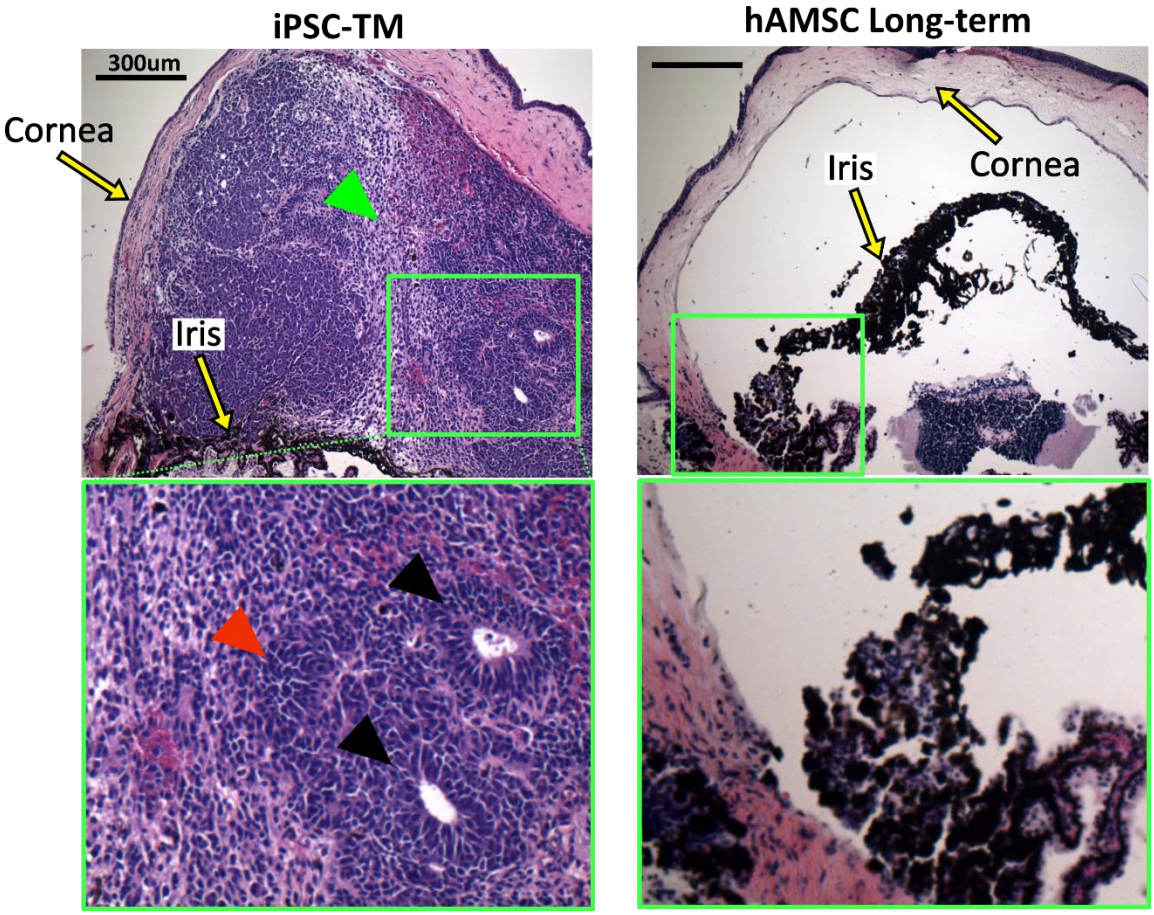

Figure 7. Histopathological assessment of tumors in eyes receiving transplanted cells. iPSC-TM- and hAMSC-transplanted eyes were stained with hematoxylin and eosin (H&E). iPSC-TM sections show distinct tumor characteristics in the anterior chamber, including the presence of rosettes (black arrowheads), densely packed cells with high nuclear-cytoplasmic ratios (red arrowhead), and more loosely coherent cells (green arrowhead). Note that eyes were collected immediately after showing visible signs of tumor growth (usually within a month post-transplantation) and not at a pre-defined time point. hAMSC eyes at long-term time point showed

no sign of tumor growth. In all panels, the green boxes provide a magnified view of the areas where tumor growth or the accumulation of exogenous cells occurred.

4. Discussion

The overarching goal of this study was to evaluate the effectiveness of a magnetic TM cell delivery technique we previously developed *(15)*. Specifically, by delivering stem cells into the eyes of a mutant myocilin mouse model of POAG and observing the effects on IOP and aqueous humor dynamics for an extended period of time, we wished to evaluate the potential of this treatment for eventual clinical translation *(33)*. We hypothesized that our targeted magnetic delivery approach would prove efficacious. A secondary goal was to compare the efficacy of two clinically relevant stem cell types: human adipose-derived mesenchymal stem cells (hAMSCs) and iPSCs that had been differentiated towards a TM cell phenotype (iPSC-TMs).

a. hAMSC delivery led to long-term IOP reduction

Our major finding was that magnetically steered delivery of hAMSCs led to a significant and sustained lowering of IOP, which could be almost entirely explained by improved function of the conventional outflow pathway. Specifically, we saw a ~27% (4.5 mmHg) IOP reduction in eyes receiving hAMSCs vs. saline (sham) injection control eyes, which was sustained for 9 months after cell delivery. This lowering of IOP was closely related to a stable ~2.8-fold increase in outflow facility in the hAMSC treatment group vs. saline injection controls. Additionally, eyes subjected to saline injection exhibited marginally higher intraocular pressures (IOPs) and lower outflow facilities on average, in comparison to the transgenic animals at baseline. However, due to the lack of statistical significance in these differences and the inherent age difference between the saline-injected animals and the non-injected controls at baseline, no conclusive inference can be drawn regarding the effect of saline injection.

Our measured IOPs were close to “expected IOPs” calculated from facility measurements, strongly suggesting that the majority of the IOP lowering effect after hAMSC delivery was due to an improvement in the function of the conventional outflow pathway.

b. There was a slight offset between measured and expected IOPs

Despite the very close correlation between measured and expected IOPs noted above, there was a small but consistent offset between these two quantities, which may be due to several factors. First, cell delivery could theoretically cause a decrease in the rate of AH formation or an increase

in the rate of uveoscleral outflow, which would lower experimentally-measured IOP. However, according to Equation 2, a change in the pressure-independent flow rate (Q) would disproportionately affect the IOP in groups with lower facility. For example, if we conservatively assume that the 1.2 mmHg average residual (Experimental IOP − Expected IOP) was caused by a difference in inflow rate for transgenic animals vs. wild-type animals, which we used as the reference for calculating inflow rate (see Methods), the 95% confidence interval on the mean of the residuals would have been ~5 times larger than what we actually calculated. The second possible explanation is that the mismatch was caused by an error in rebound tonometry, for example due to tonometer miscalibration or an anesthesia-induced drop in IOP *(34)*. However, if we assume that all groups, including WT animals, had an experimentally-measured IOP that was artifactually lower than true IOP, the pressure-independent flow rate (Q) calculated for WT animals would incorporate this effect. Thus, when this Q is used to calculate expected IOPs for groups other than WT animals, there should not be an offset between the experimental and expected IOPs, at least for groups with facilities similar to WT animals. We therefore suggest that the most plausible explanation is an inherent difference between the transgenic and WT animals, such as in the biomechanical properties of the cornea (leading to an error in the IOP read by the tonometer), in the episcleral venous pressure, or in the amount of IOP reduction due to anesthesia.

Despite some uncertainty about the minor offset between the expected and measured IOPs, the data strongly suggests that the IOP lowering caused by stem cell therapy is largely due to a restoration of function to the conventional outflow pathway.

c. hAMSC treatment led to increased TM cellularity and reduced BMM

One of the hallmarks of POAG is loss of TM cells *(5)*, which was an early motivation for TM cell therapy as a potential treatment for this disease. We found that hAMSC delivery led to a striking 2.2-fold increase in TM cellularity 3-4 weeks after treatment vs. saline-injected controls, which showed cellularities similar to eyes from WT mice. This increased cellularity declined somewhat by 3-4 months after cell injection, but then stabilized for up to 9 months after injection. Additionally, the increase in cellularity was strongly correlated with a decrease in IOP for pooled data from all the experimental groups. This correlation more directly highlights the potential of TM cell therapy in treating ocular hypertension, where TM cellularity is reduced and IOP is elevated *(5)*. Interestingly, Alvarado et al. showed that humans at birth have ~2.3-fold higher TM cellularity compared to a 40 year-old individual, and that this cellularity reduces sharply within the first five

years of life *(5)*. This trend in human eye cellularity resembles, both qualitatively and quantitatively, our observations after hAMSC treatment when the ~27-month average lifespan *(35)* of the mouse is taken into account. Further studies of factors controlling TM cellularity after hAMSC delivery are indicated but lie beyond the scope of the current study.

Another feature of POAG is an accumulation of ECM within the juxtacanalicular tissue *(36)*. The mechanism(s) underlying this ECM accumulation are not entirely understood. Nevertheless, increased levels of transforming growth factor-β2 (TGF-β2) in the AH of POAG patients *(37)* and its role in decreasing the activity of matrix metalloproteinases (MMPs) suggest that the abnormal ECM deposits may be due to decreased ECM turnover *(36, 38)*. Thus, after detecting the significant increase in TM cellularity and reduction in IOP using hAMSCs, we wondered whether transplanted cells would also affect ECM levels in the TM. Our quantification showed that this was indeed the case: hAMSC-transplanted eyes at the mid-term timepoint had 35% less basement membrane material (BMM) under the inner wall of Schlemm's canal than in saline-injected control eyes. This finding is consistent with the general theme of TM functional restoration seen throughout this study. A future study to analyze the levels of TGF-β2 in the AH as well as the ratio of active to pro-form levels of MMPs in hAMSC-transplanted eyes would be of interest to better understand the mechanism through which exogenous cells modulate ECM turnover.

d. Comparison with previous work

Unfortunately, it is not feasible to directly compare the results of this study with those of previous studies that have successfully demonstrated the efficacy of non-magnetic cell therapy in MYOC^{Y437H} mice *(9, 10)*. This is due to the unexpected lack of a POAG phenotype in our transgenic mice (discussed in detail below). Yet in our study, we found a stable IOP lowering and increase in outflow facility over 9 months (corresponding to one-third of the animals' lifespan) which for the first time attests to the possible longevity of IOP lowering due to TM cell therapy. In addition, because of the targeted nature of our delivery technique, we could achieve these reported therapeutic outcomes by injecting a total of only ~1,500 cells, which is significantly lower, i.e. more efficient, than the 50,000 cells used in previous studies *(9, 10)*.

One literature comparison that can be made is for BMM normalized length. Li et al. reported values of 0.40 [0.23, 0.57] for this quantity in naïve eyes and 0.50 [0.38, 0.60] for sham-injected (PBS containing non-conjugated polymeric nanoparticles) eyes in 2-3 months old C57BL/6 mice*(28)*. Overby et al. measured a BMM normalized length of 0.29 [0.16, 0.42] in 6-7 month old

mice from the same strain *(29)*. Despite our sham mid-term group being 9-11 months old and being on a transgenic background, with no phenotypic manifestation, the 0.52 [0.34, 0.70] BMM normalized length we measured for this group is consistent with those previously reported values. The fact that we observed reduced BMM length in cell-treated eyes vs. control values may suggest that a homeostatic balance in cell-treated eyes was tipped towards the presence of less BMM, consistent with hypotensive IOP measurements and greater outflow facility.

e. hAMSCs outperformed iPSC-TMs

This study for the first time compared the IOP-lowering performance of hAMSCs vs. iPSC-TMs – two of the most clinically relevant cell types for future TM cell therapy *(33)*. Surprisingly, we found that the performance of iPSC-TMs was significantly inferior to that of hAMSCs, as quantified by several outcome measures; most notably, the IOP reduction after iPSC-TM cell delivery was only half that seen after hAMSC delivery. The beneficial effect of iPSC-TM treatment on TM cellularity was also significantly lower than hAMSC at the short-term time point (1.4-fold vs. 2.2-fold increase), although this difference declined at the mid-term time point (1.4-fold vs. 1.6-fold increase). In addition to their IOP-reducing efficacy, another major drawback of the iPSC-TMs was the high incidence of ocular tumorigenicity. More than 60% of the eyes injected with iPSC-TM cells developed tumors, requiring termination of the experiment. A body of previous literature, including a systematic review of 1000 clinical trials involving mesenchymal stem cell transplantation, finds no incidence of tumorigenicity in tissues receiving mesenchymal stem cells, suggesting an intrinsic resistance to tumor formation once positioned in the correct niche *(18, 19)*. On the other hand, tumorigenicity remains a concern for iPSC-derivatives due to transfection with oncogenic factors, genetic aberrations during *in vitro* cultures, and contamination of transplants with undifferentiated cells *(39–41)*. Despite following a protocol to isolate differentiated iPSC-TM cells, including using a non-integrating viral vector for transfection of reprogramming factors and a commonly-used magnetic activated cell sorting approach *(41)*, there unfortunately remains a chance for contamination and reprogramming of these cells post-transplantation. Interestingly, the iris is reported to be a favorable location for organ culture and tumor formation, with 5-fold faster growth compared to subcutaneous injection, and thus has previously been considered for tumorigenicity safety studies, emphasizing the importance of rigorous iPSC processing in any future treatments involving iPSC-TM cell injection into the anterior chamber *(42–44)*.

f. Cell retention profiles differed between the two cell types

Both cell types were detectible in the anterior chamber three weeks after injection (Figure 6B), with iPSC-TM cells tending to better integrate with the TM tissue whereas the hAMSCs mostly accumulated close to, but not within, the TM. This phenomenon, which was consistently observed, may be due to the widely-reported aggregation of mesenchymal stem cells immediately post-transplantation *(45)*, which consequently prevented them from entering the deeper aspects of the TM, characterized by narrow flow channels. Note that the exogenous iPSC-TMs more directly contributed to increasing TM cellularity than did the hAMSCs due to the better integration of iPSC-TM cells into the TM. This finding complicates the interpretation of the relationship between increased TM cellularity and IOP reduction. In addition, loss of signal in long-term *in vivo* fluorescent cell tracking is inevitable *(46)* so the fluorescent signal in Figure 6 may not be marking all the exogenous cells retained in the anterior eye.

g. A likely role for paracrine signalling underlying TM cell therapy

The lack of specific hAMSC homing into the TM also provides important insight about the putative mechanism(s) by which these cells lowered IOP and improved aqueous humor dynamics. Several hypotheses address how injected cells may affect TM functional restoration: exogenous cells can either integrate with the TM and differentiate into TM-like cells, or can promote endogenous TM cell proliferation through direct contact or through their secretome. Du and colleagues, in two studies using mice, showed that TMSCs that reach the TM co-express AQP1 and CHI3L1, indicative of their differentiation into TM cells, although quantification was not performed *(11, 14)*. Zhu et al. reported a 114% increase in TM cellularity after iPSC-TM injection in MYOC^{Y437H} mice compared to saline-injected controls, yet TM-residing exogenous cells accounted for only 23% of this increase *(9)*. This finding is consistent with several studies that report the proliferative effect of exogenous cells on the TM in terms of higher Ki-67 expression and BrdU signal, as well as an increased prevalence of Nestin+ progenitor cells *(6, 9, 12)*. How this proliferation is mediated, however, is a matter of controversy. In two studies, Zhu et al. showed that iPSC-TMs induce significant proliferation of both cells from the TM5 cell line (an immortalized TM cell line) or primary TM cells carrying Ad5RSV-myocilinY437H when in co-culture, yet did not when they were co-cultured in the presence of a physical (membrane) separation between iPSC-TMs and TM cells *(9, 12)*. Interestingly, Xiong et al. conducted similar experiments with TMSCs and MyocY437H primary TM cells and observed no proliferative effect with or without contact between the cells *(14)*. On the contrary, two studies have reported the beneficial effect of injecting conditioned

media from bone marrow MSCs in hypertensive rat eyes, including a significant reduction in IOP, neuroprotection, and elevated proliferation markers in the TM *(6, 7)*. In our study, the significant lowering of IOP seen after delivery of hAMSCs and their accumulation near, but not within, the TM supports the notion that injected cells act upon the TM through their secretome. Thus, a proteomic comparison of the secretome of hAMSCs and iPSC-TMs may provide significant insight into their paracrine effect on TM functional restoration.

h. Limitations

The main limitation of this study was the lack of a POAG phenotype in our transgenic mouse colony. Even though MYOC^{Y437H} mice have previously been shown to exhibit an elevation in IOP and a decrease in both outflow facility and TM cellularity, our colony did not show any difference in those parameters compared to WT animals. While we are not certain of the cause, one possibility is that our IOP measurements were inaccurate. However, this is unlikely because of the correlation between measured IOP and outflow facility in cohorts (Figure 3C) and the fact that IOPs in our wild-type animals lay within previously reported ranges *(9, 10, 29, 47)*. It should be noted that reported IOPs for anesthetized WT C57BL/6 mice vary depending on the measurement method used, with a lower bound of ~12.5 mmHg under deep levels of injection-induced anesthesia *(48)* and an upper bound of ~20 mmHg under gas-induced extra light anesthesia *(28)*, with values close to our measurements being frequent in the literature. An alternative, and perhaps more likely, possibility is that the transgene was silenced in the original breeders of this colony. Unfortunately, this only became evident after the 6-7 month wait time required for the expected onset of the phenotype. Despite the strong effectiveness of our novel TM cell therapy technique (even in the absence of ocular hypertension), the main concern is whether cell therapy would work as effectively in a glaucomatous eye. Raghunathan et al. showed that when healthy TM cells are cultured on the ECM derived from glaucomatous TM cells, the healthy cells experience differential stiffening and altered expression profiles similar to the glaucomatous phenotype *(49)*. Therefore, a glaucomatous ECM may negatively impact the exogenous cells and curtail their therapeutic potential. Fortunately, since in our study hAMSCs did not seem to need to integrate into the TM to lower IOP, they may also not be affected by glaucomatous changes in the TM. Additionally, Goldmann's equation (Equation 2) shows that the same percentage increase in outflow facility produces a greater magnitude of IOP lowering in a hypertensive eye vs. in a normotensive eye. Therefore, evaluation of magnetically-steered hAMSC cell therapy in an alternative pre-clinical glaucoma model is indicated.

An additional limitation is that, since histology was only performed on a subset of the eyes after outflow facility measurements, it is possible that there may also have been undetected tumors in the iPSC-injected eyes reported in the IOP and outflow facility plots. This could affect the reported efficacy of the iPSC-TM cells, and further experiments comparing hADMSCs to more carefully processed iPSC-TM cells may be worthwhile.

In summary, this work shows the effectiveness of our novel magnetic TM cell therapy approach for long-term IOP reduction through functional restoration of the conventional outflow pathway. The comparison between hAMSCs and iPSC-TM cells strongly suggested the inferiority of the latter cell type in this treatment paradigm, as judged by tumorigenicity and less effective IOP lowering. The localization of injected hAMSCs deep in the iridocorneal angle, but not full integration into the TM, supports the hypothesis that exogenous cells promote TM functional restoration through paracrine signaling Therefore, even though the mouse model used in this study did not show a POAG phenotype, this treatment approach merits further study with the eventual goal of clinical translation.

5. Materials and Methods

a. Experimental design

We conducted experiments in several cohorts of mice, as follows:

- WT: wildtype hybrid mice (naïve controls)
- Tg: Tg-MYOCY437H mice, a model of POAG (see details below)
- Sham: Tg mice receiving phosphate-buffered saline (PBS, injection controls)
- hAMSC: Tg mice receiving magnetically-steered hAMSCs
- iPSC-TM: Tg mice receiving magnetically-steered iPSC-TMs

Our key outcome measures were IOP, outflow facility, TM cellularity, cell retention in the anterior segment, and ultrastructural analysis of TM ECM, with timelines as indicated in Figure 1 B. All measurements were made in *ex vivo* eyes, except for IOP, which was measured longitudinally in living mice.

After breeding and genotyping, mice were maintained to age 6-7 months, when transgenic animals were expected to have developed a POAG phenotype. We then made baseline

measurements and performed stem cell (or sham) injections, and followed animals for various durations:

- Short-term: 3-4 weeks after cell injection
- Mid-term: 3-4 months after cell injection, and
- Long-term: 9 months after cell injection.

Exogenous cell retention in the anterior chamber was measured at only the short-term timepoint. This is because in our experience (data not shown) the tracer's signal was only faintly present two months after injection *in vivo,* while signal was maintained for a longer period *in vitro*, as advertised by the manufacturer. We are unsure whether this loss of signal was caused by a loss of cell integrity or by fluorescence fading *in vivo*. Further, due to the high incidence of tumorigenicity and inferior overall effectiveness in animals receiving iPSC-TM cells, long-term measurements as well as ultrastructural analysis were not pursued for this group. We chose to perform ultrastructural analysis for hAMSC group at the mid-term time point, as this is the longest timepoint previously studied *(10)* and enables comparison with previous work.

b. Cell preparation

hAMSCs were purchased commercially (Lonza Bioscience, Walkersville, MD) and were prepared for injection as described previously *(15)*. The cells were maintained at 37° C and 5% CO_2 in α-MEM supplemented by 10% FBS and 1% penicillin and streptomycin and 2 mM L-glutamine. Cells were passaged using 0.05% trypsin (25-053-CI, Corning Inc., Corning, NY) to detach cells, followed by resuspension and seeding at 5000 cells/cm^2 in T-25 cell culture flasks. hAMSCs at 80% confluence (passages 5 or 6) were magnetically labeled by overnight incubation with 150 nm amine-coated superparamagnetic iron oxide nanoparticles (SPIONs; SA0150, Ocean NanoTech, San Diego, CA) at 25 µg/ml, followed by inspection under light microscopy to verify sufficient SPION endocytosis. Cells were then trypsinized, resuspended by addition of cell culture media, and placed in a 1.5 ml microtube. To remove insufficiently magnetized cells, a 0.25" cubic N52 neodymium magnet was placed on the side of the tube, resulting in rapid formation of a cell pellet close to the magnet. Supernatant and non-magnetic cells were then removed.

In exogenous cell retention studies, the cells remaining in the microtube were labeled using the PKH26 lipophilic dye kit (Sigma-Aldrich, St. Louis, MO) according to the manufacturer's instructions. In brief, a cell solution was prepared in the diluent component of the kit and was vigorously mixed with an equal volume of the 4 µM dye solution. After 3 minutes at room

temperature, an equal volume of FBS was added to the cell solution to stop the reaction and cells were washed 3 times with the cell culture media to remove any unbound dye. For all the experiments where animals received hAMSC, cells were then resuspended in sterile PBS to a final concentration of 1 k cells/µl.

Mouse iPSC-TMs have previously been developed and characterized *(9)*. In brief, mouse dermal fibroblasts are reprogrammed through Sendai virus-mediated reprogramming with the transcription factors OCT4, SOX2, KLF4, and c-MYC. The pluripotency of reprogrammed iPSCs was confirmed using RT-PCR, immunocytochemistry, immunoblotting, and teratoma formation. iPSCs were then differentiated by culturing in conditioned media from primary human TM (phTM) cells. To prepare this conditioned media, phTM cells were extracted from donor eyes and cultured in α-MEM supplemented by 10% inactivated FBS and 2% primocin. Conditioned media was then collected from the cells and sterilized by passing through a 0.2 µm membrane filter. The iPSCs were maintained in conditioned media for 8 weeks to induce differentiation. It is important to remove any undifferentiated iPSCs from the iPSC-TM populations due to the risk of tumorgenicity associated with pluripotent stem cells. Therefore, the iPSC-TMs were incubated with CD15 antibodies (Miltneyi Biotec, Bergisch Gladbach, Germany) conjugated with magnetic microbeads to label the undifferentiated iPSCs. Then the cells were washed, loaded into a MACS LD column and were placed in a magnetic separator (Miltenyi Biotec, Germany).

c. Transgenic mice

All animal procedures were approved by the Georgia Tech Institutional Animal Care and Use Committee and performed in conformance with the ARVO Statement for the Use of Animals in Ophthalmic and Vision Research. Breeder pairs of C57BL/6 Tg-MYOCY437H mice were shipped from Iowa to a quarantining facility (Charles River, Wilmington, MA, USA), underwent IVF rederivation, and were shipped to Georgia Tech after ~4 months. Breeders carrying one copy of the transgene on a C57BL/6 background were crossed with SJL mice (Charles River) of similar age, with half of the hybrid offspring carrying the transgene. Pups were genotyped using human MYOC primers (forward: CGTGCCTAATGGGAGGTCTAT; reverse: CTGGTCCAAGGTCAATTGGT). Only F1 animals were used in studies.

d. Cell injections

Cell injection needles were fabricated as described previously *(15)*. In brief, glass micropipettes were pulled using a pipette puller (P-97, Sutter Instruments, Novato, CA, USA) and the tips were

broken and beveled at a 30˚ on a microelectrode beveler (BV-10, Sutter Instruments, Novato, CA, USA) followed by rotating to both sides for enhanced sharpness (tri-beveling). The resulting needle had a pointed tip and an outer dimeter of approximately 100 µm. Cell adhesion to the needle walls in the lumen can cause inconsistent cell delivery to the eye; thus, we plasma cleaned the needles, coated them with trichlorosilane and loaded them with 0.02% Pluronic F-127 (P2443, Sigma-Aldrich) for 1 hr at room temperature followed by vigorously rinsing with PBS. Needles were sterilized with 70% ethanol prior to injections.

Each animal was prepared for unilateral injection of cells by applying a tropicamide eyedrop (Bausch and Lomb, Bridgewater, NJ, USA) to start pupil dilation before inducing anesthesia using an induction chamber receiving 2.5% isoflurane at 600 ml/min. Once toe-pinch reflex was lost, the animal was transferred to a heated bed and the head was immobilized with Velcro straps while anesthesia was maintained through a nose cone. A drop of tetracaine (Bausch and Lomb) was applied to the eye being injected while the contralateral eye received ophthalmic lubricant (SystaneUltra, Alcon, Geneva, Switzerland) to prevent drying. The needle, mounted on an injector assembly (MMP-KIT, WPI, Sarasota, FL, USA), was attached to a micromanipulator and connected to a microsyringe pump (PHD Ultra, Harvard Apparatus, Holliston, MA, USA). The needle was filled with 3 µl of the injection solution (either cells, or PBS for control (sham) injections), aligned at a 30° angle with the eye, and advanced into the AC in a swift motion until the tip was located approximately in the center of the AC while the eye was held in a proptosed position using a pair of non-magnetic forceps (Figure 1 A). A total of 1.5 µl of the solution was injected at 2.4 µl/min and if the solution contained cells, a point magnet (a thin stainless-steel rod attached to a permanent magnet) was used to magnetically steer the cells towards the TM in a continuous motion for the duration of cell ejection from the needle as previously described in detail *(15)*. Injected eyes received ophthalmic antibiotic combination ointment (neomycin, polymyxin, bacitracin) and were kept on a heated bed until recovery from anesthesia.

e. IOP measurements

We measured the IOPs between 1 to 3 pm (to minimize diurnal variations) by first placing the mouse in an induction chamber until the righting reflex was lost and breathing slowed. The animal was then transferred to a heated platform, secured with straps, and a tonometer (TonoLab, iCare, Vantaa, Finland) mounted on a micromanipulator (M3301, WPI, Sarasota, FL, USA) was aligned perpendicular to the corneal surface at the center of the cornea. Eight IOP measurements were taken from each eye and the reported IOP was the average of all 8 measurements. Even though

some labs exclude the highest and lowest of the 8 measurements from the IOP average *(50)*, we did not observe a significant intra-measurement variability and thus included all the 8 replicates when determining the IOP. The entire duration of IOP measurement was typically 3 minutes or less, which is less than has been reported for the start of significant anesthesia-induced IOP reduction *(34, 51)*.

f. Measurement of outflow facility

Outflow facility, which quantifies the ease of fluid drainage from the eye, is defined as the ratio of steady-state outflow rate over intraocular pressure in an enucleated eye. We measured facility in enucleated eyes using the previously established iPerfusion system *(52)*. The system's sensors were calibrated before each measurement session to ensure reliability and the absence of bubbles or leaks, which can cause large errors in the measurements. Animals were euthanized by intraperitoneal injection of sodium pentobarbital and eyes were enucleated by sliding a pair of fine angled forceps behind the eye through the nasal side of the eye socket and pulling the eye out by grabbing onto the optic nerve and the surrounding retrobulbar tissues. The posterior of the eye was secured to a mounting post using a very small drop of cyanoacrylate adhesive (Superglue) inside a heated water bath (35°C) filled with DPBS supplemented with 5.5 mM glucose. A beveled micropipette, mounted on a micromanipulator, was then used to cannulate the eye at a 30° angle. The eyes were stabilized at an IOP of 8 mmHg for 30 minutes and then perfused at 8 evenly distributed pressure steps starting from 4.5 mmHg and finishing at 16.5 mmHg while flow rate and pressure data were acquired (Figure 3 Ai-iii). The resulting flow-pressure data were fit with an empirical power-law relationship *(52)*

$$C(P) = C_r \left(\frac{P}{P_r}\right)^{\beta} \tag{1}$$

where C is the steady-state outflow facility calculated for each pressure step, P is the steady state pressure for that step, and the subscript r refers to the parameter evaluated at the reference pressure of 8 mmHg which corresponds to the physiologic pressure difference across the conventional outflow pathway *(52)*. β is a non-linearity parameter that is determined by data fitting along with C_r. A total of 114 eyes were randomly chosen for outflow facility measurements, of which, 9 were excluded due to failed perfusion (e.g., poor cannulation).

g. Comparison between experimental and expected IOP

Steady-state AH dynamics can be described by the modified Goldmann equation *(27)*:

$$Q = Q_{in} - Q_0 = C(IOP - P_e) \quad (2)$$

where Q_{in} is the rate of AH humor formation, Q_0 is the uveoscleral (unconventional) outflow rate, and P_e is the episcleral venous pressure. Since the left-hand side of Equation 2 is essentially pressure-independent, Q was assumed to be the same across all the experimental groups.

To cross-validate the IOP and outflow facility measurements, we calculated Q in wildtype animals by inserting the mean measured outflow facility and mean measured IOP from wildtype animals into Equation 2, assuming P_e to be 7 mmHg *(52)*. Average outflow facilities for all the groups were then adjusted using Equation 1 to account for the pressure-dependence of facility. Using these adjusted facilities and assuming Q to be the same for all groups, we calculated an "expected IOP" for each experimental group, which can be interpreted as the IOP that is consistent with the measured outflow facility.

h. Histology, histopathology, and morphometric studies

Similar to the procedure used previously *(15)*, all experimental eyes were immersion fixed in 10% formalin (Fisher Healthcare, Waltham, MA, USA) overnight at 4°C after the corresponding *in vivo* and *ex vivo* measurements (no measurements were performed on the eyes used for exogenous cell retention study). Of these eyes, a total of 59 were randomly selected from various groups for TM cellularity quantifications. Eyes were then dissected under a surgical microscope and isolated anterior segments were cut into four leaflets. This anterior segment wholemount was placed on a glass side with the cornea facing up and mounted with PBS. A Leica DMB6 epifluorescent microscope (Leica Microsystems, Wetzlar, Germany) was used to create fluorescent *en face* tilescan images. Two quadrants of each wholemount were then prepared for cryosectioning. These quadrants received sequential 15 minute treatments in 15% sucrose (Sigma-Aldrich, St. Louis, MO, USA), 30% sucrose, and a 1:1 solution of 30% sucrose and optimal cutting temperature (OCT) media. After embedding in OCT, samples were floated in a 100% ethanol bath cooled by dry ice to flash freeze. 10 µm-thick sagittal sections were cut using a CryoStar NX70 cryostat (ThermoFisher Scientific, Waltham, MA, USA) and placed on Superfrost gold plus slides (ThermoFisher Scientific, Waltham, MA, USA). In an additional step, specific to TM cellularity

quantification, the samples were permeabilized with 0.2% Triton X-100 for 10 minutes and stained with DAPI (NucBlue fixed cell DAPI, Invitrogen, Waltham, MA, USA) for 15 minutes followed by coverslipping with antifade media (Prolong Diamond antifade medium, Invitrogen, Waltham, MA, USA). Sagittal sections were then imaged as tilescans.

To quantify TM cellularity, ideally all the cells in the TM should be counted. However, due to partial or complete collapse of the Schlemm's canal and the small separation between the TM and the iris in the murine iridocorneal angle *(53)*, identifying the boundaries of the TM can be challenging. Thus, to minimize error, we instead counted the DAPI-stained nuclei in the region that we could identify as the TM with a high confidence and normalized this count by the length of the inner wall of Schlemm's canal adjacent to this segment (Figure 4 A). Note that morphological characteristics such as the autofluorescence in the corneoscleral shell, high degree of pigmentation in the iris, as well as the change in the density and orientation of the cells transitioning from the TM to iris helped with locating the TM cell nuclei.

Eyes of animals injected with iPSC-TMs showing anatomical signs of tumor growth were enucleated and immersion fixed in 10% formalin for histopathological studies. Three of these eyes were randomly chosen, dehydrated, and embedded in paraffin. Subsequently, 5 µm thick sagittal sections were cut using a microtome (ThermoFisher Scientific, Waltham, MA, USA) and stained with hematoxylin and eosin (H&E). Three additional eyes from hAMSC long-term group underwent the same procedure for comparison.

i. Quantification of ECM underlying the inner wall of SC

The amount of basement membrane material (BMM) in the hAMSC mid-term experimental group and in corresponding injection control eyes (four eyes in each cohort) were quantified using electron micrographs, using an approach similar to that previously described *(28, 29)*. In brief, the two anterior segment quadrants not used for TM cell counting (described above) were immersion fixed overnight at 4°C in universal fixative (2.5% glutaraldehyde, 2.5% paraformaldehyde in Sörensen's buffer). The specimens were next embedded in Epon resin, and 65-nm sagittal sections were cut through iridocorneal tissues using an ultramicrotome (Leica EM UC6, A-1170; Leica Mikrosysteme GmbH) followed by staining with uranyl acetate/lead citrate. Sagittal sections were examined with a JEM-1400 electron microscope (JEOL USA, Peabody, MA) at 8000x magnification. At least one section per quadrant was included in the quantification of basement membrane material (BMM) deposits as described below.

The lengths of BMM segments directly in contact with the inner wall of Schlemm's canal (IW) and the total length of IW were measured from electron micrographs using ImageJ *(54)*by two independent annotators in a masked fashion. To enhance BMM identification from micrographs, we first adjusted the contrast for each image, using an ImageJ macro that assigned a brightness level of 255 to a manually-selected region of the lumen of SC and a brightness level of zero to a manually-selected region of a cell nucleus. The ratio of the length of BMM segments directly underlying the IW to the total length of IW was calculated for each segment, representing the extent of non-fenestrated BMM material underlying the IW. Supplementary Supplementary Figure 1 exhibits an example of the demarcations. Note that ECM deposits clearly separated from the IW were not considered as BMM deposits.

j. Statistical analysis

IOP, outflow facility, and TM cellularity index were tested for normality using the Shapiro-Wilk test for each treatment group. Since outflow facility is known to be log-normally distributed *(52)*, facility data was first log-transformed prior to conducting any statistical tests. All outcome measures, except for TM cellularity and normalized BMM length, were analyzed by one-way ANOVA. For TM cellularity and BMM length, we used a linear mixed-effects model, treating the experimental group as the fixed effect while considering the eyes, various sections of each eye, and annotators (for BMM only) as replicates, i.e. as random effects. Following these analyses, we conducted *post hoc* comparisons with Bonferroni correction. However, we limited our comparisons to those chosen *a priori* to be relevant to the interpretation of our study to avoid an overly conservative adjustment of critical p-values as required by Bonferroni correction. To compare the impact of different treatments on IOP and outflow facility, we computed the difference between the treatment groups and their respective injection controls. Subsequently, we conducted two-tailed t-tests with Bonferroni correction. Given the log-transformation of facility data, the subtracted values became ratios upon inverse transformation. To check for consistency between IOP and outflow facility measurements, we calculated residuals as the difference between the expected and experimentally-measured IOPs. A two-tailed t-test was then performed on these residuals with $H_0: \mu = 0$. Pearson correlation test was used measure the relation between TM cellular density and IOP. All analyses were done using MATLAB (v2020, MathWorks, Natick, MA, USA). A significance level of 5% was employed for all tests, unless explicitly stated otherwise.

6. References

1. Y.-C. Tham, X. Li, T. Y. Wong, H. A. Quigley, T. Aung, C.-Y. Cheng, Global prevalence of glaucoma and projections of glaucoma burden through 2040: a systematic review and meta-analysis. *Ophthalmology* **121**, 2081–2090 (2014).

2. A. L. Coleman, S. Miglior, Risk factors for glaucoma onset and progression. *Surv. Ophthalmol.* **53**, S3–S10 (2008).

3. G. Reardon, S. Kotak, G. F. Schwartz, Objective assessment of compliance and persistence among patients treated for glaucoma and ocular hypertension: a systematic review. *Patient Prefer. Adherence* , 441–463 (2011).

4. A. Heijl, M. C. Leske, B. Bengtsson, L. Hyman, B. Bengtsson, M. Hussein, E. M. G. T. Group, Reduction of intraocular pressure and glaucoma progression: results from the Early Manifest Glaucoma Trial. *Arch. Ophthalmol.* **120**, 1268–1279 (2002).

5. J. Alvarado, C. Murphy, R. Juster, Trabecular Meshwork Cellularity in Primary Open-angle Glaucoma and Nonglaucomatous Normals. *Ophthalmology* **91**, 564–579 (1984).

6. R. Manuguerra-Gagné, P. R. Boulos, A. Ammar, F. A. Leblond, G. Krosl, V. Pichette, M. R. Lesk, D.-C. Roy, Transplantation of mesenchymal stem cells promotes tissue regeneration in a glaucoma model through laser-induced paracrine factor secretion and progenitor cell recruitment. *Stem Cells* **31**, 1136–1148 (2013).

7. C. Roubeix, D. Godefroy, C. Mias, A. Sapienza, L. Riancho, J. Degardin, V. Fradot, I. Ivkovic, S. Picaud, F. Sennlaub, Intraocular pressure reduction and neuroprotection conferred by bone marrow-derived mesenchymal stem cells in an animal model of glaucoma. *Stem Cell Res. Ther.* **6**, 1–13 (2015).

8. D. W. Abu-Hassan, X. Li, E. I. Ryan, T. S. Acott, M. J. Kelley, Induced Pluripotent Stem Cells Restore Function in a Human Cell Loss Model of Open-Angle Glaucoma. *Stem Cells* **33**, 751–761 (2015).

9. W. Zhu, O. W. Gramlich, L. Laboissonniere, A. Jain, V. C. Sheffield, J. M. Trimarchi, B. A. Tucker, M. H. Kuehn, Transplantation of iPSC-derived TM cells rescues glaucoma phenotypes in vivo. *Proc. Natl. Acad. Sci.* **113**, E3492–E3500 (2016).

10. W. Zhu, A. Jain, O. W. Gramlich, B. A. Tucker, V. C. Sheffield, M. H. Kuehn, Restoration of aqueous humor outflow following transplantation of iPSC-derived trabecular meshwork cells in a transgenic mouse model of glaucoma. *Invest. Ophthalmol. Vis. Sci.* **58**, 2054–2062 (2017).

11. H. Yun, Y. Wang, Y. Zhou, A. Kumar, K. Wang, M. Sun, D. B. Stolz, X. Xia, C. R. Ethier, Y. Du, Human stem cells home to and repair laser-damaged trabecular meshwork in a mouse model. *Commun. Biol.* **1**, 216 (2018).

12. W. Zhu, C. R. Godwin, L. Cheng, T. E. Scheetz, M. H. Kuehn, Transplantation of iPSC-TM stimulates division of trabecular meshwork cells in human eyes. *Sci. Rep.* **10**, 2905 (2020).

13. Y. Zhou, X. Xia, E. Yang, Y. Wang, K. G. Marra, C. R. Ethier, J. S. Schuman, Y. Du, Adipose-derived stem cells integrate into trabecular meshwork with glaucoma treatment potential. *FASEB J. Off. Publ. Fed. Am. Soc. Exp. Biol.* **34**, 7160 (2020).

14. S. Xiong, A. Kumar, S. Tian, E. E. Taher, E. Yang, P. R. Kinchington, X. Xia, Y. Du, M. Pera, M. E. Bronner, Eds. Stem cell transplantation rescued a primary open-angle glaucoma mouse model. *eLife* **10**, e63677 (2021).

15. M. R. Bahrani Fard, J. Chan, G. Sanchez Rodriguez, M. Yonk, S. R. Kuturu, A. T. Read, S. Y. Emelianov, M. H. Kuehn, C. R. Ethier, Improved magnetic delivery of cells to the trabecular meshwork in mice. *Exp. Eye Res.* **234**, 109602 (2023).

16. X. Wang, Q. Cao, S. Wu, M. R. Bahrani Fard, N. Wang, J. Cao, W. Zhu, Magnetic Nano-Platform Enhanced iPSC-Derived Trabecular Meshwork Delivery and Tracking Efficiency. *Int. J. Nanomedicine* **17**, 1285–1307 (2022).

17. B. M. Braunger, B. Ademoglu, S. E. Koschade, R. Fuchshofer, T. G. B'Ann, J. A. Kiland, E. A. Hennes-Beann, K. G. Brunner, P. L. Kaufman, E. R. Tamm, Identification of adult stem cells in Schwalbe's line region of the primate eye. *Invest. Ophthalmol. Vis. Sci.* **55**, 7499–7507 (2014).

18. M. M. Lalu, L. McIntyre, C. Pugliese, D. Fergusson, B. W. Winston, J. C. Marshall, J. Granton, D. J. Stewart, Safety of Cell Therapy with Mesenchymal Stromal Cells (SafeCell): A Systematic Review and Meta-Analysis of Clinical Trials. *PLOS ONE* **7**, e47559 (2012).

19. D. E. Rodríguez-Fuentes, L. E. Fernández-Garza, J. A. Samia-Meza, S. A. Barrera-Barrera, A. I. Caplan, H. A. Barrera-Saldaña, Mesenchymal Stem Cells Current Clinical Applications: A Systematic Review. *Arch. Med. Res.* **52**, 93–101 (2021).

20. Q. J. Ding, W. Zhu, A. C. Cook, K. R. Anfinson, B. A. Tucker, M. H. Kuehn, Induction of trabecular meshwork cells from induced pluripotent stem cells. *Invest. Ophthalmol. Vis. Sci.* **55**, 7065–7072 (2014).

21. H. Friedman, N. Ator, N. Haigwood, W. Newsome, J. S. Allan, T. G. Golos, J. H. Kordower, R. E. Shade, M. E. Goldberg, M. R. Bailey, P. Bianchi, The Critical Role of Nonhuman Primates in Medical Research. *Pathog. Immun.* **2**, 352–365 (2017).

22. T. Acott, J. R. Samples, J. M. Bradley, D. R. Bacon, S. S. Bylsma, E. M. Van Buskirk, Trabecular Repopulation by Anterior Trabecular Meshwork Cells After Laser Trabeculoplasty: Reply. *Am. J. Ophthalmol.* **108**, 210 (1989).

23. R. M. Sappington, B. J. Carlson, S. D. Crish, D. J. Calkins, The Microbead Occlusion Model: A Paradigm for Induced Ocular Hypertension in Rats and Mice. *Invest. Ophthalmol. Vis. Sci.* **51**, 207–216 (2010).

24. J. C. Morrison, C. G. Moore, L. M. Deppmeier, B. G. Gold, C. K. Meshul, E. C. Johnson, A rat model of chronic pressure-induced optic nerve damage. *Exp. Eye Res.* **64**, 85–96 (1997).

25. A. J. Turner, R. Vander Wall, V. Gupta, A. Klistorner, S. L. Graham, DBA/2J mouse model for experimental glaucoma: pitfalls and problems. *Clin. Experiment. Ophthalmol.* **45**, 911–922 (2017).

26. G. S. Zode, M. H. Kuehn, D. Y. Nishimura, C. C. Searby, K. Mohan, S. D. Grozdanic, K. Bugge, M. G. Anderson, A. F. Clark, E. M. Stone, V. C. Sheffield, Reduction of ER stress via a chemical chaperone prevents disease phenotypes in a mouse model of primary open angle glaucoma. *J. Clin. Invest.* **121**, 3542–3553 (2011).

27. R. F. Brubaker, Goldmann's equation and clinical measures of aqueous dynamics. *Exp. Eye Res.* **78**, 633–637 (2004).

28. G. Li, C. Lee, A. T. Read, K. Wang, J. Ha, M. Kuhn, I. Navarro, J. Cui, K. Young, R. Gorijavolu, Anti-fibrotic activity of a rho-kinase inhibitor restores outflow function and intraocular pressure homeostasis. *Elife* **10**, e60831 (2021).

29. D. R. Overby, J. Bertrand, O.-Y. Tektas, A. Boussommier-Calleja, M. Schicht, C. R. Ethier, D. F. Woodward, W. D. Stamer, E. Lütjen-Drecoll, Ultrastructural Changes Associated With Dexamethasone-Induced Ocular Hypertension in Mice. *Invest. Ophthalmol. Vis. Sci.* **55**, 4922–4933 (2014).

30. C. R. Ethier, R. D. Kamm, B. A. Palaszewski, M. C. Johnson, T. M. Richardson, Calculations of flow resistance in the juxtacanalicular meshwork. *Invest. Ophthalmol. Vis. Sci.* **27**, 1741–1750 (1986).

31. F. J. Wippold, A. Perry, Neuropathology for the Neuroradiologist: Rosettes and Pseudorosettes. *AJNR Am. J. Neuroradiol.* **27**, 488–492 (2006).

32. M. J. Moore, J. A. Sebastian, M. C. Kolios, Determination of cell nucleus-to-cytoplasmic ratio using imaging flow cytometry and a combined ultrasound and photoacoustic technique: a comparison study. *J. Biomed. Opt.* **24**, 106502 (2019).

33. S. J. Coulon, J. S. Schuman, Y. Du, M. R. B. Fard, C. R. Ethier, W. D. Stamer, A novel glaucoma approach: Stem cell regeneration of the trabecular meshwork. *Prog. Retin. Eye Res.* **90**, 101063 (2022).

34. Y. Qiu, H. Yang, B. Lei, Effects of three commonly used anesthetics on intraocular pressure in mouse. *Curr. Eye Res.* **39**, 365–369 (2014).

35. T. G. Graber, L. Ferguson-Stegall, J.-H. Kim, L. V. Thompson, C57BL/6 Neuromuscular Healthspan Scoring System. *J. Gerontol. A. Biol. Sci. Med. Sci.* **68**, 1326–1336 (2013).

36. R. Fuchshofer, U. Welge-Lussen, E. Lütjen-Drecoll, The effect of TGF-β2 on human trabecular meshwork extracellular proteolytic system. *Exp. Eye Res.* **77**, 757–765 (2003).

37. R. C. Tripathi, J. Li, W. F. Chan, B. J. Tripathi, Aqueous humor in glaucomatous eyes contains an increased level of TGF-beta 2. *Exp. Eye Res.* **59**, 723–727 (1994).

38. E. R. Tamm, R. Fuchshofer, What Increases Outflow Resistance in Primary Open-angle Glaucoma? *Surv. Ophthalmol.* **52**, S101–S104 (2007).

39. S. Neri, Genetic Stability of Mesenchymal Stromal Cells for Regenerative Medicine Applications: A Fundamental Biosafety Aspect. *Int. J. Mol. Sci.* **20**, 2406 (2019).

40. N. Lamm, U. Ben-David, T. Golan-Lev, Z. Storchová, N. Benvenisty, B. Kerem, Genomic Instability in Human Pluripotent Stem Cells Arises from Replicative Stress and Chromosome Condensation Defects. *Cell Stem Cell* **18**, 253–261 (2016).

41. S. Yamanaka, Pluripotent Stem Cell-Based Cell Therapy-Promise and Challenges. *Cell Stem Cell* **27**, 523–531 (2020).

42. L. Olson, Å. Seiger, Brain tissue transplanted to the anterior chamber of the eye. *Z. Für Zellforsch. Mikrosk. Anat.* **135**, 175–194 (1972).

43. E. Inagaki, E. Arai, S. Hatou, T. Sayano, H. Taniguchi, K. Negishi, Y. Kanai, Y. Sato, H. Okano, K. Tsubota, S. Shimmura, The Anterior Eye Chamber as a Visible Medium for In Vivo Tumorigenicity Tests. *Stem Cells Transl. Med.* **11**, 841–849 (2022).

44. C. W. Boone, L. T. DuPree, Quantitative tumorigenicity assays using the anterior chamber of the mouse eye. *Cancer Res.* **28**, 1734–1737 (1968).

45. A. J. Burand Jr, L. Di, L. K. Boland, D. T. Boyt, M. V. Schrodt, D. A. Santillan, J. A. Ankrum, Aggregation of human mesenchymal stromal cells eliminates their ability to suppress human T cells. *Front. Immunol.* **11**, 143 (2020).

46. F. Progatzky, M. J. Dallman, C. Lo Celso, From seeing to believing: labelling strategies for in vivo cell-tracking experiments. *Interface Focus* **3**, 20130001 (2013).

47. H. Yun, K. L. Lathrop, E. Yang, M. Sun, L. Kagemann, V. Fu, D. B. Stolz, J. S. Schuman, Y. Du, A Laser-Induced Mouse Model with Long-Term Intraocular Pressure Elevation. *PLOS ONE* **9**, e107446 (2014).

48. S. W. John, J. R. Hagaman, T. E. MacTaggart, L. Peng, O. Smithes, Intraocular pressure in inbred mouse strains. *Invest. Ophthalmol. Vis. Sci.* **38**, 249–253 (1997).

49. V. K. Raghunathan, J. Benoit, R. Kasetti, G. Zode, M. Salemi, B. S. Phinney, K. E. Keller, J. A. Staverosky, C. J. Murphy, T. Acott, J. Vranka, Glaucomatous cell derived matrices differentially modulate non-glaucomatous trabecular meshwork cellular behavior. *Acta Biomater.* **71**, 444–459 (2018).

50. C. M. McDowell, K. Kizhatil, M. H. Elliott, D. R. Overby, J. van Batenburg-Sherwood, J. C. Millar, M. H. Kuehn, G. Zode, T. S. Acott, M. G. Anderson, Consensus recommendation for mouse models of ocular hypertension to study aqueous humor outflow and its mechanisms. *Invest. Ophthalmol. Vis. Sci.* **63**, 12–12 (2022).

51. S. Tsuchiya, T. Higashide, S. Hatake, K. Sugiyama, Effect of inhalation anesthesia with isoflurane on circadian rhythm of murine intraocular pressure. *Exp. Eye Res.* **203**, 108420 (2021).

52. J. M. Sherwood, E. Reina-Torres, J. A. Bertrand, B. Rowe, D. R. Overby, Measurement of outflow facility using iPerfusion. *PloS One* **11**, e0150694 (2016).

53. G. Li, C. Lee, V. Agrahari, K. Wang, I. Navarro, J. M. Sherwood, K. Crews, S. Farsiu, P. Gonzalez, C.-W. Lin, A. K. Mitra, C. R. Ethier, W. D. Stamer, In vivo measurement of trabecular meshwork stiffness in a corticosteroid-induced ocular hypertensive mouse model. *Proc. Natl. Acad. Sci. U. S. A.* **116**, 1714–1722 (2019).

54. C. A. Schneider, W. S. Rasband, K. W. Eliceiri, NIH Image to ImageJ: 25 years of image analysis. *Nat. Methods* **9**, 671–675 (2012).

55. N. Sadeghiani, L. S. Barbosa, L. P. Silva, R. B. Azevedo, P. C. Morais, Z. G. M. Lacava, Genotoxicity and inflammatory investigation in mice treated with magnetite nanoparticles surface coated with polyaspartic acid. *J. Magn. Magn. Mater.* **289**, 466–468 (2005).

56. A. Stroh, C. Zimmer, C. Gutzeit, M. Jakstadt, F. Marschinke, T. Jung, H. Pilgrimm, T. Grune, Iron oxide particles for molecular magnetic resonance imaging cause transient oxidative stress in rat macrophages. *Free Radic. Biol. Med.* **36**, 976–984 (2004).

57. N. Singh, G. J. S. Jenkins, R. Asadi, S. H. Doak, Potential toxicity of superparamagnetic iron oxide nanoparticles (SPION). *Nano Rev.* **1**, 5358 (2010).

7. Acknowledgements

Funding

National Institutes of Health grant R01 EY030071 (CRE, SYE, MHK)

The Georgia Research Alliance (CRE).

Author Contributions

Conceptualization: CRE, MRBF, MHK, SYE

Methodology: MRBF, CRE, MHK, LC, JC, ATR, GL, AJ, HEG, WDS, BNS, SMS

Investigation: MRBF, CRE

Visualization: MRBF, CRE

Funding acquisition: CRE, MHK, SYE

Project administration: CRE, MRBF

Supervision: CRE

Writing – original draft: MRBF, CRE

Writing – review & editing: MRBF, JC, ATR, GL, LC, BNS, SMS, AJ, HEG, SYE, WDS, MHK, CRE

8. List of supplementary materials

S.1 Supplementary figures

Supplementary Figure 1. Quantification procedure for the amount of basement membrane materials (BMM) underlying to the inner wall of Schlemm's canal.

Supplementary Figure 2. Complementary micrographs to Figure 4 used for TM cellularity quantifications.

Supplementary Figure 3. Autofluorescence from various ocular tissues at the same fluorescence settings as used in Figure 6.

Supplementary Figure 4. Prussian blue staining to locate SPIONs within the anterior segment after cell transplantation.

S.2 SPION visualization post-transplantation

S.2.1 Prussian blue staining of SPIONs

S.2.2 SPIONs co-located with exogenous cells post-transplantation

S.2.3 SPIONs did not accumulate within the native tissues of the AC

SUPPLEMENTARY MATERIALS

S.1 Supplementary figures

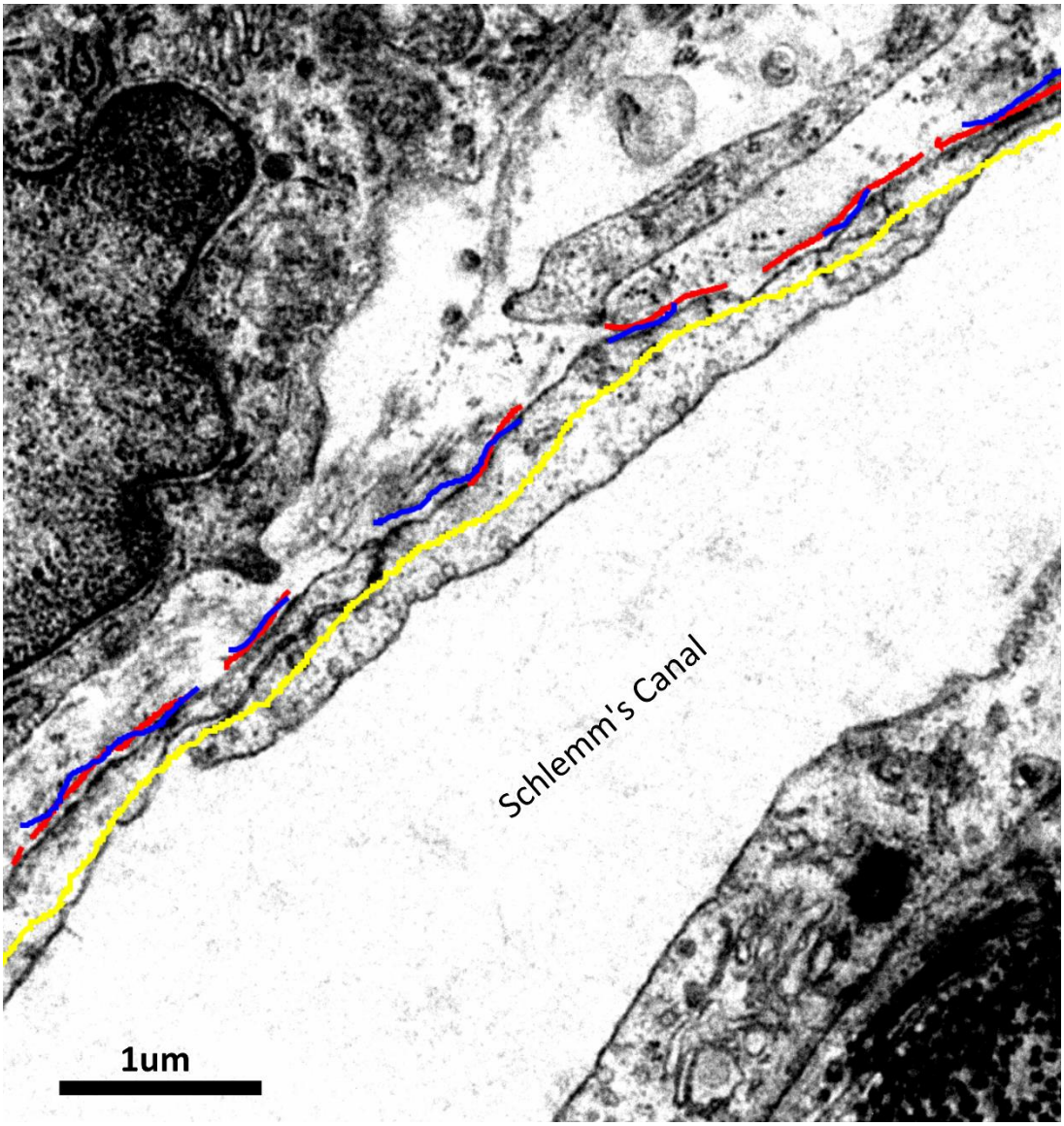

Supplementary Figure 1. Quantification procedure for the amount of basement membrane materials (BMM) underlying to the inner wall of Schlemm's canal. The red and blue line segments mark the basement membrane materials adjacent to the inner wall of Schlemm's canal for each annotator. The summed length of these segments was then normalized by the overall length of

the inner wall (yellow) for quantifications. The yellow line is slightly shifted from the blue and red segments for easier visualization.

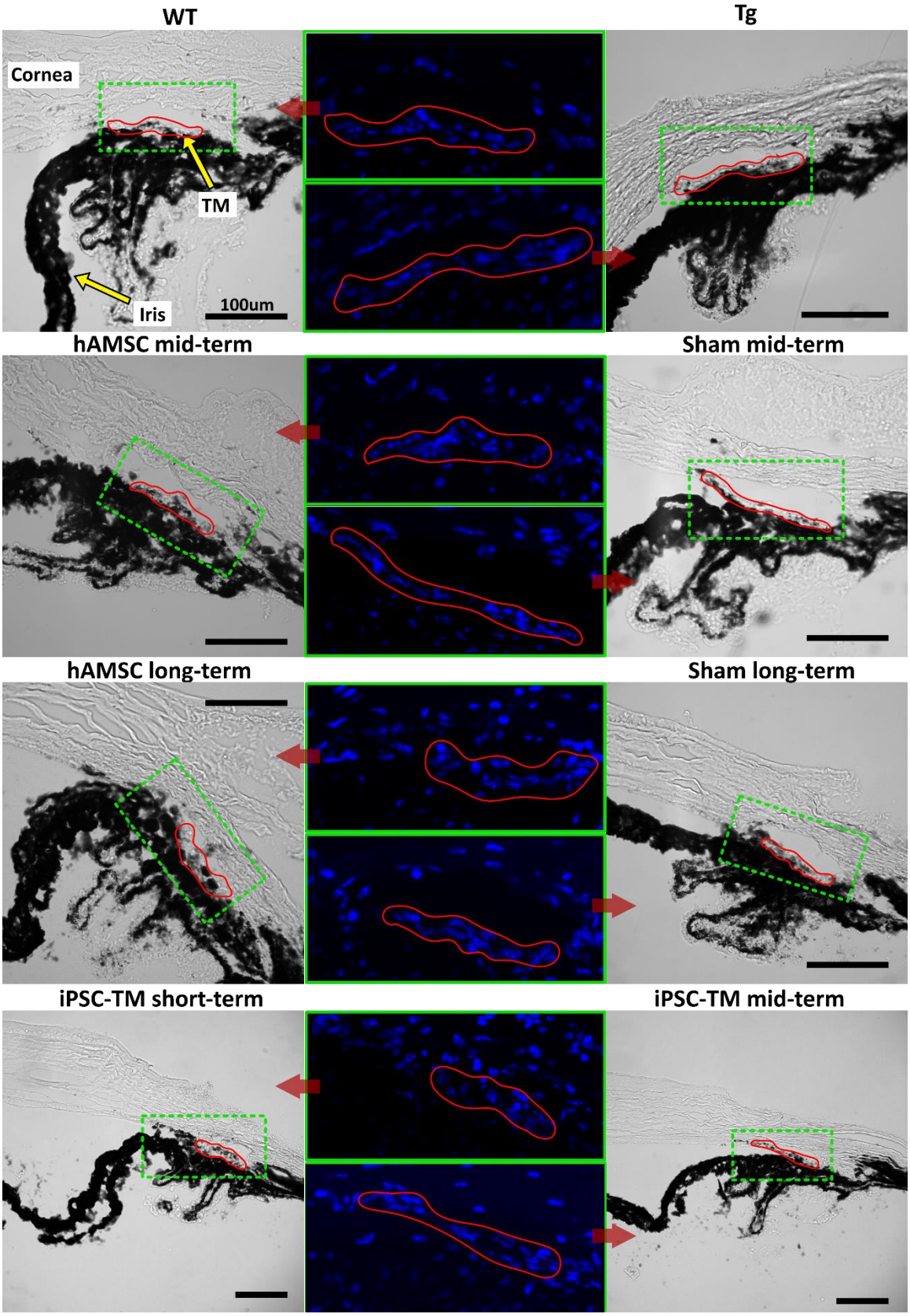
WT
Tg
Cornea
TM
Iris
100um
hAMSC mid-term
Sham mid-term
hAMSC long-term
Sham long-term
iPSC-TM short-term
iPSC-TM mid-term

927

Supplementary Figure 2. Complementary micrographs to Figure 4 used for TM cellularity quantifications. Overview micrographs are shown in the left and right columns (see labels above images), with zoomed regions in the central column as indicated by the red arrows. Regions of interest (ROI), encompassing the parts of TM used for nuclei counting (demarcated in red) are outlined by green dashed boxes and the DAPI-stained nuclei (blue) are shown in a zoomed-in fluorescent micrograph of the ROI (green solid box). In overview images in which the ROI is tilted, the corresponding fluorescent micrograph has been rotated counterclockwise so that it is horizontal, thus enabling a more compact presentation.

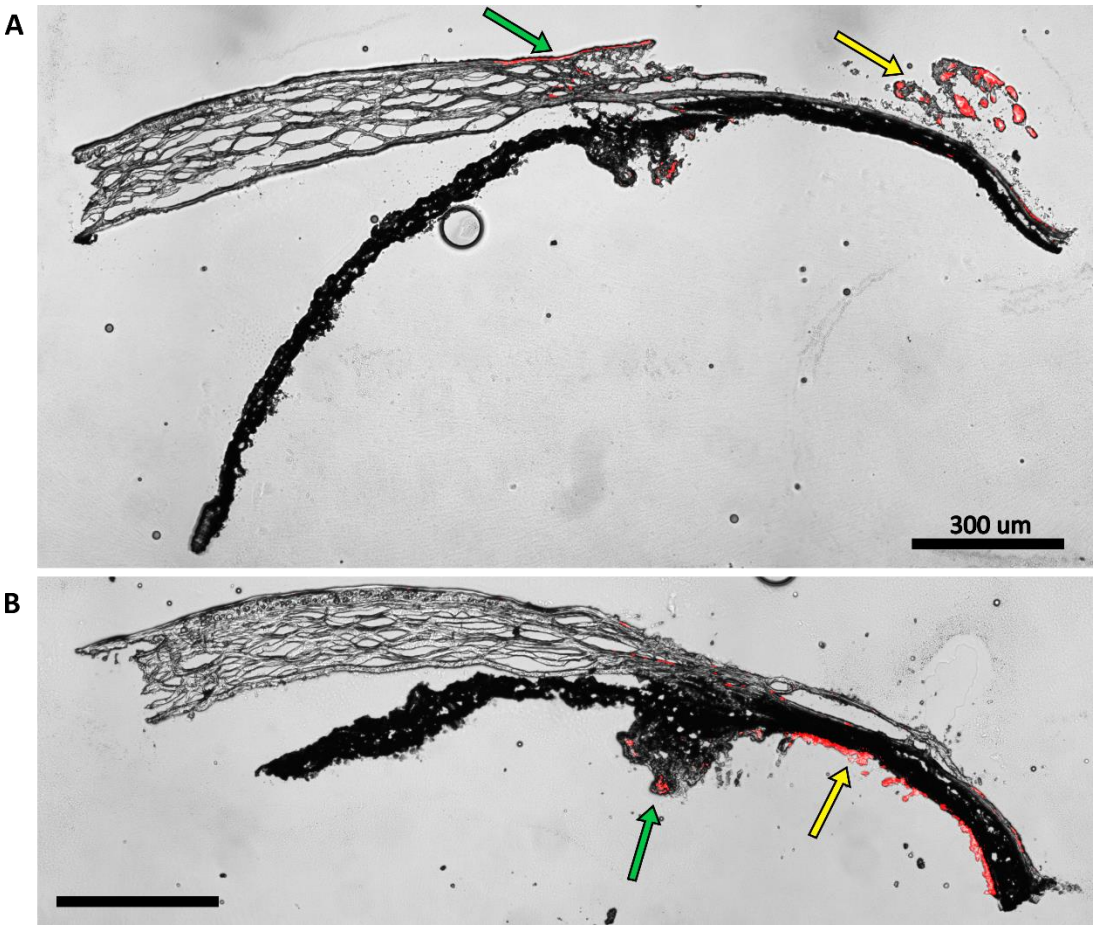

Supplementary Figure 3. Autofluorescence from various ocular tissues at the same fluorescence settings as used in Figure 6. The autofluorescence profile is dependent on the quality of dissection. In A, a signal is evident in insufficiently removed orbital tissue (yellow arrow) and at the limbus (green arrow). In B, autofluorescence is localized within the remnants of the retina (yellow arrow) and ciliary body (green arrow).

S.2 SPION visualization post-transplantation

For reasons described below, it was useful to know where SPIONs had accumulated within the eye. We therefore carried out histological analyses of tissue sections to visualize SPIONs, Using a Prussian blue staining process.

S.2.1 Prussian blue staining of SPIONs

A Prussian blue solution was freshly prepared by mixing a 1:1 ratio of a 20% aqueous solution of hydrochloric acid and a 10% aqueous solution of potassium ferrocyanide (K4Fe(CN)6·3H2O, Sigma-Aldrich). Cryosections from the eyes which were sampled for cell retention studies were rehydrated for 30 minutes. Subsequently, the sections were covered with the 10% potassium ferrocyanide solution for 5 minutes, followed by a 15-minute treatment with the Prussian blue solution. After treatment, the sections were rinsed three times in distilled water, dehydrated through increasing concentrations of ethanol, cleared in xylene, and then mounted for imaging.

S.2.2 SPIONs co-located with exogenous cells post-transplantation

A major concern regarding the use of SPIONs for cell encapsulation is dose-dependent toxicity which could damage both the transplanted cells and native tissues *(55, 56)*. We therefore visualized the SPIONs using Prussian blue staining anterior segment sagittal sections (Supplementary Supplementary Figure 4). Unfortunately, this dark blue stain proved barely discernable from pigment. Detectible labeling could mostly be found at comparable locations within the AC as in hAMSC-injected eyes (Figure 6B), where both the cells and SPIONs accumulated in the vicinity of TM, and in iPSC-TM-injected eyes (Figure 6B), with the cells and SPIONs found within the TM. Prussian blue did not stain materials in the saline-injected control eyes.

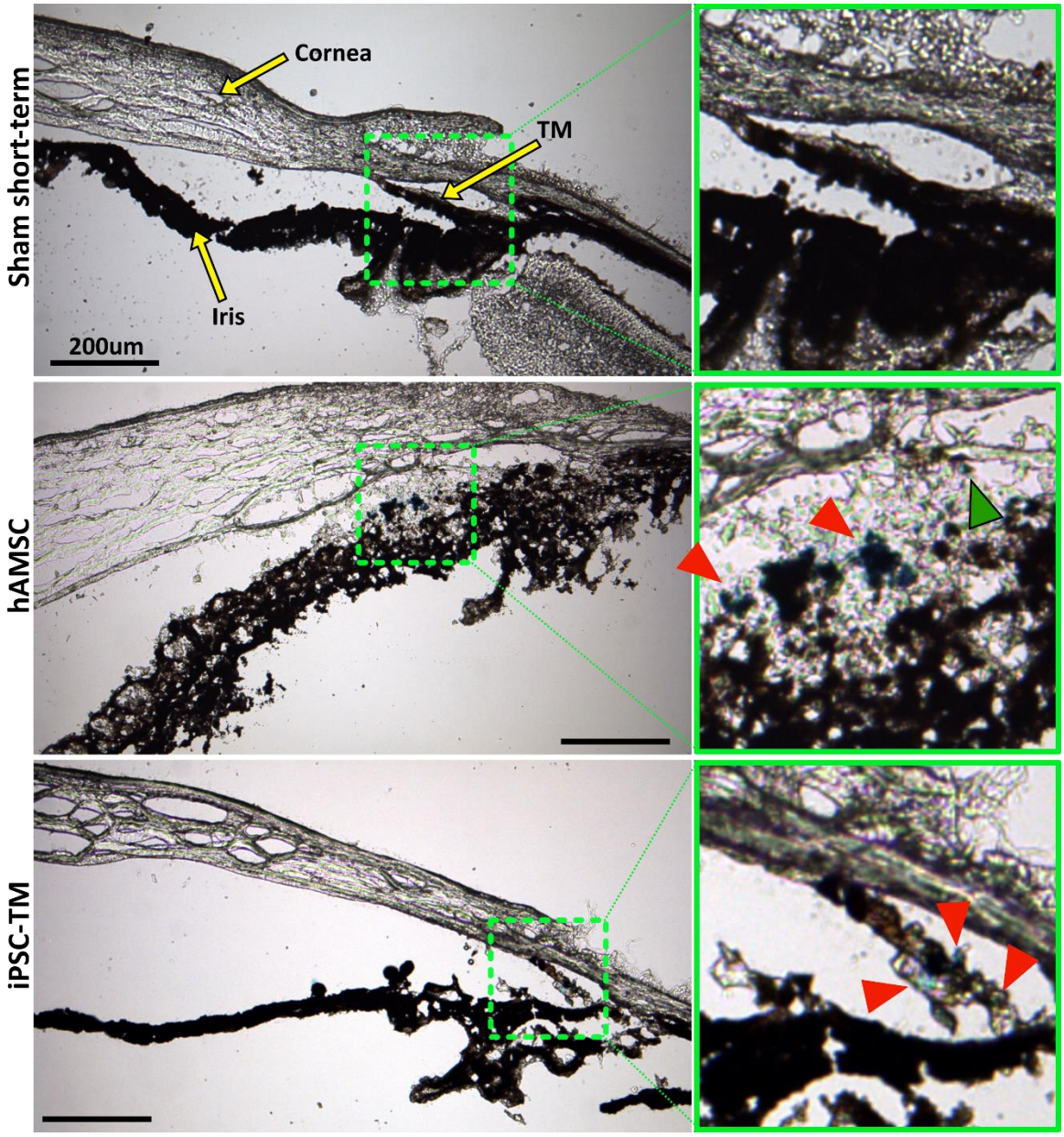

Supplementary Figure 4. Prussian blue staining to locate SPIONs within the anterior segment after cell transplantation. The left column shows overview images of the anterior segment, while green boxes in the right column show a zoomed view of the region with strongest Prussian blue staining, corresponding to the green dashed boxes in the left column. Top row: No Prussian blue staining could be found in the saline injection control. Middle row: Prussian blue stain is challenging to distinguish from melanin, but accumulation of blue label (red arrowheads) can be seen to coincide with the locations of exogenous cells visualized in Figure 6. In particular, injected hAMSCs primarily accumulated close to the TM, corresponding to the location of Prussian blue stain. A small region of Prussian blue staining can be observed in the TM (green arrowhead). Bottom row: Similarly, in eyes receiving iPSC-TMs, most of the Prussian blue staining was found within the TM, corresponding to the location of injected cells (Figure 6). Unfortunately, the fluorescent signal in Figure 6 was significantly attenuated after Prussian blue staining and could

not be overlaid on these images to assist with interpretation. Iris degradation, notable in the middle row, is an undesirable artifact of the cryosectioning or staining process (Figure 6).

S.2.3 SPIONs did not accumulate within the native tissues of the AC

Iron oxide-induced toxicity, both as cytotoxicity and genotoxicity, is a major concern when using SPIONs in cell encapsulation and transplantation. *In vitro* studies have reported that SPION labeling is generally safe at concentrations below 100 µg/ml *(57)*. Since we used a four-fold lower concentration for cell labeling in this study, the encapsulated cells were likely unaffected.

Once inside the AC, the SPIONs may be released from the injected cells. The TM, as the phagocytic and filtering component of the main AH outflow pathway, is a likely destination. Our Prussian blue staining to visualize SPIONs in the AC after delivery was masked by pigmentation and was hard to visualize (Supplementary Supplementary Figure 4). The SPIONs that we could detect were mostly co-located with the transplanted cells and were likely not released at a significant rate within the AC. In the case of iPSC-TM cells, which showed good integration with the TM, detectable SPIONs were also primarily found within the TM. Whether these SPIONs had been released from the injected cells or were still encapsulated remains unknown. Nevertheless, the significant increase in TM cellularity discussed above indicates that accumulation of SPIONs within the TM is unlikely to have any toxic effect on native tissues.

Table 1. Outcome measures, shown as means and [95% confidence intervals].

Group	IOP (mmHg)	Facility (nl/min/mmHg)	Cellular Density (nuclei/μm)
WT	15.6 [14.8,16.3]	4.4 [3.7,5.2]	0.24 [0.15,0.33]
Tg	15.4 [14.7,16.1]	3.8 [3.3,4.4]	0.28 [0.23,0.32]
Sham Short	17.1 [16.0,18.1]	3.2 [2.3,4.3]	0.27 [0.20,0.34]
MSC Short	12.8 [11.9,13.8]	8.4 [6.3,11.2]	0.58 [0.42,0.73]
Sham Mid	16.9 [15.5,18.2]	3.0 [2.1,4.3]	0.24 [0.18,0.31]
MSC Mid	12.4 [11.6,13.2]	8.4 [7.1,9.9]	0.40 [0.34,0.47]
Sham Long	16.7 [16.0,17.5]	3.4 [2.8,4.2]	0.23 [0.17,0.28]
MSC Long	12.2 [11.0,13.3]	8.0 [5.9,10.9]	0.37 [0.31,0.43]
iPSC-TM Short	14.8 [14.0,15.6]	4.3 [3.0,6.2]	0.36 [0.27,0.45]
iPSC-TM Mid	15.0 [14.3,15.7]	4.3 [3.6,5.1]	0.34 [0.21,0.47]

Table 2. Result of multiple comparison for various groups and variables, with statistically significant comparisons highlighted in orange*.

	Compared groups		p-values		
	Vs.		IOP	Facility	Cellular
1	WT	Tg	0.3579	0.1353	0.6264
2	Tg	Sham Short	0.0070	0.0901	0.9214
3	Tg	Sham Mid	0.0311	0.0614	0.2879
4	Tg	Sham Long	0.0652	0.1865	0.2442
5	Sham Short	hAMSC Short	<0.0001	<0.0001	<0.0001
6	Sham Short	iPSC-TM Short	0.0006	0.0692	0.0535
7	hAMSC Short	hAMSC Mid	0.2786	0.4838	<0.0001
8	hAMSC Short	hAMSC Long	0.2111	0.4045	<0.0001
9	hAMSC Short	iPSC-TM Short	0.0013	0.0019	<0.0001
10	Sham Mid	hAMSC Mid	<0.0001	<0.0001	<0.0001
11	Sham Mid	iPSC-TM Mid	0.0047	0.0210	0.0072
12	hAMSC Mid	hAMSC Long	0.3497	0.3719	0.5595
13	hAMSC Mid	iPSC-TM Mid	<0.0001	<0.0001	0.2751
14	Sham Long	hAMSC Long	<0.0001	<0.0001	0.0020
15	iPSC-TM Short	iPSC-TM Mid	0.3597	0.4877	0.8516

* Post-hoc comparisons were performed after ANOVA (for IOP and outflow facility) or linear mixed-effect model (for TM cellularity). Bonferroni correction was used to adjust the critical p-value from 0.05 to 0.0033 (based on the 15 reported comparisons).